

Multi-IRS-Enabled Integrated Sensing and Communications

Yuan Fang, Siyao Zhang, Xinmin Li, Jie Xu, and Shuguang Cui

Abstract

This paper studies a multi-intelligent-reflecting-surface-(IRS)-enabled integrated sensing and communications (ISAC) system, in which multiple IRSs are installed to help the base station (BS) provide ISAC services at separate line-of-sight (LoS) blocked areas. We focus on the scenario with semi-passive uniform linear array (ULA) IRSs for sensing, in which each IRS is integrated with dedicated sensors for processing echo signals, and each IRS simultaneously serves one sensing target and one communication user (CU) in its coverage area. In particular, we suppose that the BS sends combined information and dedicated sensing signals for ISAC, and we consider two cases with point and extended targets, in which each IRS aims to estimate the direction-of-arrival (DoA) of the corresponding target and the complete target response matrix, respectively. Under this setup, we first derive the closed-form Cramér-Rao bounds (CRBs) for parameters estimation under the two target models. For the point target case, the CRB for AoA estimation is shown to be inversely proportional to the cubic of the number of sensors at each IRS, while for the extended target case, the CRB for target response matrix estimation is proportional to the number of IRS sensors. Next, we consider two different types of CU receivers that can and cannot cancel the interference from dedicated sensing signals prior to information decoding. To achieve fair and optimized sensing performance, we minimize the maximum CRB at all IRSs for the two target cases, via jointly optimizing the transmit beamformers at the BS and the reflective beamformers at the multiple IRSs, subject to the minimum signal-to-interference-plus-noise ratio (SINR) constraints at individual CUs, the maximum transmit power constraint at the BS, and the unit-modulus constraints at

Y. Fang is with the Future Network of Intelligence Institute (FNii) and the School of Science and Engineering (SSE), The Chinese University of Hong Kong (Shenzhen), Shenzhen, 518172, China (e-mail: fangyuan@cuhk.edu.cn).

S. Zhang is with the School of Computer Science and Technology, Southwest University of Science and Technology, Mianyang 621000, China, and the FNii, The Chinese University of Hong Kong (Shenzhen), Shenzhen, 518172, China (e-mail: zsy@mails.swust.edu.cn).

X. Li is with the School of Information Engineering, Southwest University of Science and Technology, Mianyang 621000, China, and the FNii, The Chinese University of Hong Kong (Shenzhen), Shenzhen, 518172, China (e-mail: lixm@swust.edu.cn).

J. Xu and S. Cui are with SSE and FNii, The Chinese University of Hong Kong (Shenzhen), Shenzhen, 518172, China (e-mail: xujie@cuhk.edu.cn, shuguangcui@cuhk.edu.cn). J. Xu is the corresponding author.

the multiple IRSs. To tackle the highly non-convex SINR-constrained max-CRB minimization problems, we propose efficient algorithms based on alternating optimization and semi-definite relaxation, to obtain converged solutions. Finally, numerical results are provided to verify the benefits of our proposed designs over various benchmark schemes based on separate or heuristic beamforming designs.

Index Terms

Integrated sensing and communications (ISAC), semi-passive intelligent reflecting surfaces (IRS), Cramér-Rao bound (CRB), joint transmit and reflective beamforming.

I. INTRODUCTION

Integrated sensing and communications (ISAC) has been recognized as one of the usage scenarios for future sixth-generation (6G) wireless networks [1], [2], in which the spectrum resources, wireless infrastructures, and radio signals are reused for the dual role of radar sensing and wireless communications. On the one hand, ISAC allows the cellular base stations (BSs) and mobile devices to jointly design the transmit signals and waveforms to perform both sensing and communications, thus properly managing the co-channel interference between them and accordingly enhancing the resource utilization efficiency. On the other hand, ISAC can also enable the coordination between sensing and communications, such that the sensing information can be exploited to facilitate communications by, e.g., reducing the conventional training overhead, and the communications among different nodes can be utilized to support networked sensing from different views in a large scale [3]. As such, ISAC is expected to significantly improve the sensing and communication performances for supporting various new applications such as auto-driving, extended reality, and unmanned aerial vehicles (UAVs) [4]. To make ISAC a reality, extensive research efforts have been devoted to studying innovative ISAC system designs such as the waveform and beamforming optimization (see [5], [6] and the references therein). However, due to the complicated radio propagation environments, the practical ISAC performance may degrade seriously when the transmission links are blocked by obstacles such as trees and buildings.

Intelligent reflecting surface (IRS) provides a viable solution to enhance both sensing and communication performances by reconfiguring the radio environments via reflecting the incident signals with properly controlled phases and/or amplitudes [7]–[9]. In particular, IRSs can be used in wireless communications networks to help enhance the signal coverage, increase the desired signal strength, mitigate the undesired interference, reshape the communication channel

rank, and accordingly boost the communication performance [10]–[12]. Furthermore, IRSs can also be employed in wireless sensing systems to create virtual line-of-sight (LoS) links to see targets in the non-line-of-sight (NLoS) regions, provide multi-view sensing for facilitating the target detection and estimation, and enable networked target localization [13].

While there have been extensive works investigating IRS-enabled wireless communications [14], there have been only a handful of prior works studying IRS-enabled sensing [15], [16] and IRS-enabled ISAC [17]–[20]. First, the IRS-enabled sensing can be generally implemented in two different ways, namely the passive IRS sensing [15] and semi-passive IRS sensing [16], in which the IRS is not and is installed with the dedicated sensors for signal reception, such that the sensing signal processing is implemented at the BS remotely and at the IRS directly, respectively. In particular, the authors in [15] studied the passive IRS sensing for estimating the target angle with respect to the IRS based on the echo signals over the BS-IRS-target-IRS-BS link. In [15], the authors first analyzed the Cramér-Rao bounds (CRBs) for the BS to estimate the angle of point target or the target response matrix of extended target, and then proposed to jointly optimize the active transmit beamforming and the passive reflective beamforming to minimize the CRBs. By contrast, the authors in [16] studied the semi-passive IRS sensing for localizing the targets close to the IRS by using the echo signals over the BS-IRS-target-IRS link, in which the IRS passive reflection matrix was optimized to maximize the received echo signal power at the IRS. Next, the works [18]–[20] considered the IRS-enabled ISAC by considering passive IRS sensing, and [17] studied the ISAC scenario with an IRS assisting the communications only. In particular, by considering the passive IRS sensing, the work [18] maximized the minimum reflected beampattern gains towards multiple sensing angles with respect to the IRS by jointly optimizing the transmit and reflective beamforming. In [19], the authors studied a scenario where the target sensing is corrupted by multiple clutters with signal-dependent interference, in which the radar signal-to-interference-plus-noise ratio (SINR) was maximized. The work [20] proposed to jointly design the communication and sensing waveform to minimize the total transmit power at BS while ensuring the constraints on both communication and radar SINR as well as the cross-correlation pattern design requirements. However, the above prior works on IRS-enabled sensing and IRS-enabled ISAC mainly focused on the case with one single IRS, which has a limited coverage area due to the round-trip pathloss. In practice, each BS may have multiple sensing coverage holes due to the distributed obstructions. Therefore, it is important to exploit multiple IRSs to cooperate in helping BS cover different LoS blocked areas.

In the literature, the multi-IRS-enabled wireless communications have been extensively studied, in which multiple IRSs are deployed for enhancing the coverage areas via either independent single-hop reflections [21]–[23] or cooperative multi-hop reflections [24]–[27]. For instance, the authors in [21] studied a downlink multi-IRS multi-user communication system with each IRS serving one user, in which the joint beamforming was optimized to maximize the minimum SINR among all users. The work [22] studied a downlink wireless communication system with multiple distributed IRSs, in which the on-off control at the IRSs were optimized jointly with the resource allocation to maximize the system energy efficiency while ensuring the minimum achievable rate requirements at the users. The authors in [23] further investigated the impact of secondary reflections in an uplink multi-IRS-aided multi-user communication system, in which the passive beamforming at these IRSs were optimized to maximize the weighted-sum rate or the minimum rate at multiple users. Furthermore, the authors in [24] studied the IRS-enabled multi-reflection between a BS and multiple users, in which the active beamforming at the BS and the passive beamforming at multiple IRSs were jointly designed based on deep reinforcement learning. In addition, [25] investigated a multi-route multi-hop cascaded IRS communication system, with the objective of maximizing achievable sum rate at the multiple users via joint design of active and cascaded passive beamforming. In [26] and [27], the authors studied the optimal multi-IRS-reflection path selection for multi-IRS beam routing problem. On the other hand, multiple IRSs can be employed to enhance the signal coverage of BS via single reflection of each IRS. Despite the research progress, the above prior works only studied the multi-IRS-enabled wireless communications. To our best knowledge, how to efficiently implement multi-IRS-enabled sensing and multi-IRS-enabled ISAC has not been well investigated in the literature yet. This thus motivates our investigation in this work.

This paper studies the multi-IRS-enabled ISAC system, in which multiple IRSs are deployed at different locations to assist the BS to provide seamless ISAC services via their single reflections.¹ The multi-IRS-enabled ISAC is expected to enhance the coverage areas of both sensing and communications with reduced hardware and operational costs [28]. However, as compared to the single-IRS-enabled counterpart, the multi-IRS-enabled ISAC introduces new technical challenges due to the involvement of multiple IRSs. In particular, as the same transmit signals from the BS

¹How to use multi-reflection or multi-hop links of multiple IRSs for sensing and ISAC is also an interesting direction, which, however, is beyond the scope of this paper and is left for future work.

need to be reflected by different IRSs to serve their respective areas, it is difficult to quantify the fundamental target sensing performances (e.g., for target estimation or target detection) at different IRSs. Furthermore, as there are multiple IRSs associated with one BS, how to coordinate the reflective beamforming at all the IRSs together with the transmit optimization at the BS is also an important but difficult task.

More specifically, this paper investigates the multi-IRS-enabled ISAC system consisting of one BS and multiple semi-passive IRSs each equipped with a uniform linear array (ULA), in which each IRS employs reflective beamforming to serve one communication user (CU) and sense one target at the same time. To facilitate ISAC, the BS sends dedicated sensing signals combined with information signals. As the dedicated sensing signals can be known *a priori*, we consider two different types of CU receivers that are and are not able to cancel the interference caused by the sensing signals, respectively. Besides, we also consider two cases with point and extended targets, for which each IRS aims to estimate the direction-of-arrival (DoA) of its corresponding target, and the complete response matrix between each IRS and its corresponding target, respectively. The main results of this paper are summarized as follows.

- First, different from most prior works on IRS-enabled ISAC that used the transmit beam pattern and radar SINR as the sensing performance measures, we consider the CRB for target estimation as the metric to characterize the fundamental sensing performance, which serves as the variance lower bound of any practical biased estimators [6], [15]. In particular, for the point and extended targets, we derive the closed-form CRB for estimating the target DoA and the complete target response matrix, respectively. The derived CRB for DoA estimation is shown to be inversely proportional to the cubic of the number of sensors at each IRS for the point target case, and the CRB for target response matrix estimation is proportional to the number of sensors at each IRS for the extended target case.
- Then, under the two target models and by considering two different CU types, we minimize the maximum CRB for targets estimation at all IRSs to achieve fair and optimized sensing performance, via jointly optimizing the transmit beamformers at the multiple BS and the reflective beamformers at the IRSs, subject to the minimum SINR constraints at individual CUs, the maximum transmit power constraint at the BS for transmit beamforming, and the unit-modulus constraints at the IRSs for reflective beamforming. The four SINR-constrained max-CRB minimization problems are highly non-convex due to the coupling of transmit beamforming at BS and passive beamforming at IRSs as well as the unit-modulus

constraints. To tackle these problems, we propose efficient algorithms to obtain converged solutions based on alternating optimization and semi-definite relaxation (SDR).

- Finally, numerical results show that our proposed designs perform close to the sensing performance upper bound (or CRB lower bound) by the sensing only design, and outperform various benchmark schemes based on transmit beamforming only or with zero-forcing (ZF) beamforming. It is also shown that the sensing signal interference cancellation is essential in further enhancing the ISAC performance.

The rest of the paper is organized as follows. Section II presents the multi-semi-passive-IRS-enabled ISAC system model. Section III derives the closed-form estimation CRBs for both point and extended target cases. Section IV and Section V present the joint transmit and reflective beamforming solutions to the SINR constrained max-CRB minimization problems for the cases with point and extended targets, respectively. Section VI presents numerical results to validate the performance of our proposed joint beamforming designs as compared to other benchmarks. Finally, Section VII concludes the paper.

Notations: The circularly symmetric complex Gaussian (CSCG) distribution with mean $\boldsymbol{\mu}$ and covariance \mathbf{A} is denoted as $\mathcal{CN}(\boldsymbol{\mu}, \mathbf{A})$. The notations $(\cdot)^T$, $(\cdot)^*$, $(\cdot)^H$, and $\text{tr}(\cdot)$ denote the transpose, conjugate, conjugate-transpose, and trace operators, respectively. \mathbf{I}_L stands for the identity matrix of size $L \times L$. $\text{Re}(\cdot)$ and $\text{Im}(\cdot)$ denote the real and imaginary parts of the argument, respectively. $|\cdot|$ and $\arg\{\cdot\}$ denote the absolute value and angle of a complex element, respectively. $\text{vec}(\cdot)$ denotes the vectorization operator, $\mathbb{E}(\cdot)$ denotes the expectation operation, and $\text{diag}(\mathbf{x})$ denotes a diagonal matrix with the diagonal entries specified by vector \mathbf{x} . $\text{rank}(\mathbf{X})$ denotes the rank value of matrix \mathbf{X} and $[\cdot]_{l,p}$ denotes the (l, p) -th element of a matrix. j denotes the imaginary unit. $\mathcal{A} \setminus a$ denotes the set after removing the element a in \mathcal{A} .

II. SYSTEM MODEL

We consider a multi-IRS-enabled ISAC system as shown in Fig. 1, which consists of an ISAC BS with M antennas and K semi-passive IRSs. Each IRS is equipped with a ULA of N reflecting elements and N_s receive antenna elements for sensing. Let $\mathcal{K} = \{1, \dots, K\}$ denote the set of IRSs and $\mathcal{N} = \{1, \dots, N\}$ denote the set of elements at each IRS. In practice, the coverage of each IRS is limited, and thus we assume that each IRS is deployed to provide ISAC coverage at one separate area by ignoring the interference across different areas [29]. Furthermore, it is assumed that there are one sensing target and one signal-antenna CU at the coverage area of

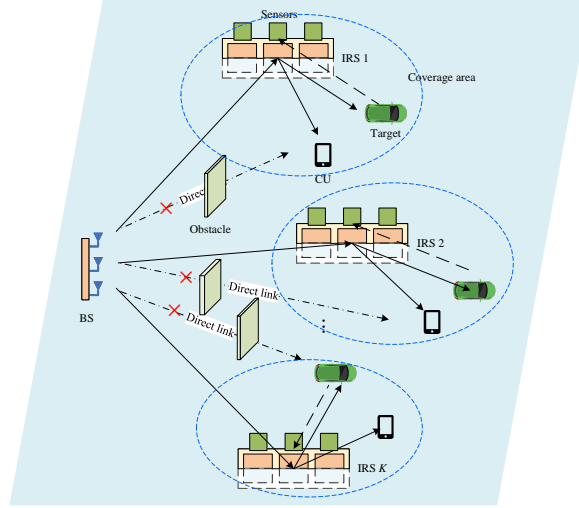


Fig. 1. The multi-semi-passive-IRS-enabled ISAC system.

each IRS, and the direct links between the BS and the targets/CUs are blocked as assumed in prior work [16].

We consider the quasi-static channel model, in which the wireless channels remain unchanged over the transmission block of interest. Let T denote the block duration or the radar dwell time. Let $\mathbf{G}_k \in \mathbb{C}^{N \times M}$ denote the channel matrix between the BS and IRS k , and $\mathbf{h}_k \in \mathbb{C}^{N \times 1}$ denote the channel vector between IRS k and the CU, which are assumed to be known by the system via proper channel estimation (see, e.g., [30]).

We consider the transmit beamforming at the BS and the reflective beamforming at the IRSs. In particular, the BS sends combined information and sensing signals to facilitate ISAC [5], [6]. Let $s_k[t]$ denote the information signal for CU k at time symbol t , and $\mathbf{w}_k \in \mathbb{C}^{M \times 1}$ denote the corresponding transmit beamforming vector. Then, the information signal vector for all CUs is denoted as $\mathbf{s}[t] = [s_1[t], \dots, s_K[t]]^T$ with $\mathbf{s}[t] \sim \mathcal{CN}(\mathbf{0}, \mathbf{I}_K)$. Let $\mathbf{s}_0[t] \in \mathbb{C}^{M \times 1}$ denote the dedicated sensing signal, which is randomly generated independent of $\mathbf{s}[t]$, with zero mean and covariance matrix $\mathbf{R}_0 = \mathbb{E}(\mathbf{s}_0[t]\mathbf{s}_0^H[t]) \approx \frac{1}{T} \sum_{t=1}^T \mathbf{s}_0[t]\mathbf{s}_0^H[t] \succeq 0$.² By combining the information and sensing signals, the transmit signal at the BS is $\mathbf{x}[t] = \sum_{k \in \mathcal{K}} \mathbf{w}_k s_k[t] + \mathbf{s}_0[t]$, for which the covariance matrix is given by $\mathbf{R}_x = \sum_{k \in \mathcal{K}} \mathbf{W}_k + \mathbf{R}_0$, where $\mathbf{W}_k = \mathbf{w}_k \mathbf{w}_k^H$ with $\text{rank}(\mathbf{W}_k) = 1$ and $\mathbf{W}_k \succeq 0$. By letting P_{sum} denote the maximum transmit power at the BS, then we have the maximum

²The statistical and sample covariance matrices are assumed to be approximately the same by considering T to be sufficiently large.

transmit power constraint at the BS as $\mathbb{E}(\|\mathbf{x}[t]\|^2) = \text{tr}(\mathbf{R}_x) = \text{tr}(\sum_{k \in \mathcal{K}} \mathbf{W}_k + \mathbf{R}_0) \leq P_{\text{sum}}$. Furthermore, we consider that each IRS k can adaptively adjust the reflection coefficients of its elements based on the channel conditions. Let $\boldsymbol{\phi}_k = [\phi_{k,1}, \dots, \phi_{k,n}, \dots, \phi_{k,N}]^T$ denote the complex reflection coefficients imposed by IRS k , where $|\phi_{k,n}| = 1$ and $\arg\{\phi_{k,n}\} \in (0, 2\pi]$, $\forall n \in \{1, \dots, N\}$.

First, we consider the wireless communication from the BS to the CUs assisted by the IRSs. By omitting the direct link from the BS to each CU k , the received signal by CU k through the BS-IRS k -CU k link at symbol t is

$$\begin{aligned}
y_k[t] &= \mathbf{h}_k^H \boldsymbol{\Phi}_k \mathbf{G}_k \mathbf{x}[t] + z_k[t] \\
&= \underbrace{\mathbf{h}_k^H \boldsymbol{\Phi}_k \mathbf{G}_k \mathbf{w}_k s_k[t]}_{\text{User's desired signal}} + \underbrace{\sum_{k' \in \mathcal{K} \setminus k} \mathbf{h}_k^H \boldsymbol{\Phi}_k \mathbf{G}_k \mathbf{w}_{k'} s_{k'}[t]}_{\text{Inter-user interference}} \\
&\quad + \underbrace{\mathbf{h}_k^H \boldsymbol{\Phi}_k \mathbf{G}_k \mathbf{s}_0[t]}_{\text{Dedicated sensing signal interference}} + z_k[t], \tag{1}
\end{aligned}$$

where $\boldsymbol{\Phi}_k = \text{diag}(\boldsymbol{\phi}_k)$, and $z_k[t] \sim \mathcal{CN}(0, \sigma^2)$ denotes the additive white Gaussian noise (AWGN) at CU k that may include the background interference among different IRSs. As the sensing signal $\mathbf{s}_0[t]$ can be generated offline, it can be known prior to transmission. As such, we consider two different types of CU receivers depending on whether they have the capability of cancelling the interference by sensing signals $\mathbf{s}_0[t]$.

- **Type-I CU receiver:** Such CU receivers do not have the capability of canceling the interference by $\mathbf{s}_0[t]$ and thus treat such interference as noise. In this case, the received SINR of CU k is

$$\begin{aligned}
\gamma_k^{(\text{I})}(\{\mathbf{W}_k\}, \{\boldsymbol{\Phi}_k\}, \mathbf{R}_0) &= \\
&= \frac{\mathbf{h}_k^H \boldsymbol{\Phi}_k \mathbf{G}_k \mathbf{W}_k \mathbf{G}_k^H \boldsymbol{\Phi}_k^H \mathbf{h}_k}{\sum_{k' \in \mathcal{K} \setminus k} \mathbf{h}_k^H \boldsymbol{\Phi}_k \mathbf{G}_k \mathbf{W}_{k'} \mathbf{G}_k^H \boldsymbol{\Phi}_k^H \mathbf{h}_k + \mathbf{h}_k^H \boldsymbol{\Phi}_k \mathbf{G}_k \mathbf{R}_0 \mathbf{G}_k^H \boldsymbol{\Phi}_k^H \mathbf{h}_k + \sigma_k^2}. \tag{2}
\end{aligned}$$

- **Type-II CU receiver:** Such CU receivers are dedicated designed for ISAC, which can cancel the interference from $\mathbf{s}_0[t]$ before decoding information signal $s_k[t]$. In this case, the received SINR of CU k is

$$\gamma_k^{(\text{II})}(\{\mathbf{W}_k\}, \{\boldsymbol{\Phi}_k\}) = \frac{\mathbf{h}_k^H \boldsymbol{\Phi}_k \mathbf{G}_k \mathbf{W}_k \mathbf{G}_k^H \boldsymbol{\Phi}_k^H \mathbf{h}_k}{\sum_{k' \in \mathcal{K} \setminus k} \mathbf{h}_k^H \boldsymbol{\Phi}_k \mathbf{G}_k \mathbf{W}_{k'} \mathbf{G}_k^H \boldsymbol{\Phi}_k^H \mathbf{h}_k + \sigma_k^2}. \tag{3}$$

Next, we consider the target estimation at the IRSs. In particular, we consider two cases with point and extended targets, which are introduced in detail as follows.

1) *Point Target Case*: Each point target is assumed to have a small spatial range and can be viewed as a far apart unstructured point for the IRS. In this case, the round-trip target response matrix from IRS k to its corresponding target to IRS k is given by

$$\hat{\mathbf{E}}_k = \beta_k \tilde{\mathbf{a}}(\theta_k) \mathbf{a}_k^T(\theta_k), \quad (4)$$

where β_k denotes the complex coefficient accounting for the radar cross-section of the target and the round-trip path-loss, $\mathbf{a}_k(\theta_k)$ denotes the array steering vector of reflecting elements at IRS k with DoA θ_k and $\tilde{\mathbf{a}}_k(\theta_k)$ denotes the steering vector at the sensors of IRS k . Here, we have

$$\mathbf{a}_k(\theta_k) = [1, e^{j\frac{2\pi}{\lambda}d \sin(\theta_k)}, \dots, e^{j\frac{2\pi}{\lambda}(N-1)d \sin(\theta_k)}]^T, \quad (5)$$

$$\tilde{\mathbf{a}}_k(\theta_k) = [1, e^{j\frac{2\pi}{\lambda}d_s \sin(\theta_k)}, \dots, e^{j\frac{2\pi}{\lambda}(N_s-1)d_s \sin(\theta_k)}]^T, \quad (6)$$

where λ denotes the carrier wavelength, and d and d_s denote the spacing of consecutive reflection elements and sensor elements at IRS k , respectively. In this case, the complex coefficient β_k and the target DoA θ_k are unknown parameters to be estimated at each IRS k .

2) *Extended Target Case*: Extended target refers to an object or an entity that occupies an area rather than being represented as a single point [31]. Unlike a point target that is typically modeled as a single point in space, an extended target can be an object with non-negligible size, such as a vehicle or a group of targets [32]. The echo signal from an extended target consists of multiple scatterers within the target volume and varies depending on its size, shape, orientation, and material properties. As a result, the point target model in (4) only reflects a single point scatterer behavior, but is not suitable to characterize extended targets. For tractable theoretical analysis, we use $\hat{\mathbf{E}}_k \in \mathbb{C}^{N_s \times N}$ to denote the complete target response matrix from IRS k to extended target to IRS k , which reflects the comprehensive effect of all scatterers within the target volume. In this case, the complete target response matrix $\hat{\mathbf{E}}_k$ corresponds to the parameters to be estimated at each IRS k .

Based on the two target models, we consider the target sensing at each semi-passive IRS k by using its dedicated sensors for receiving the echo signals reflected by the targets [16]. In

particular, the received echo signal at the sensors of each IRS k from target k at time symbol t is

$$\bar{\mathbf{y}}_k[t] = \hat{\mathbf{E}}_k \Phi_k \mathbf{G}_k \mathbf{x}[t] + \bar{\mathbf{z}}_k[t], \quad (7)$$

where $\bar{\mathbf{z}}_k[t] \sim \mathcal{CN}(\mathbf{0}, \sigma_s^2 \mathbf{I}_{N_s})$ denotes the AWGN at the sensor receiver of IRS k . By defining $\mathbf{X} = [\mathbf{x}[1], \dots, \mathbf{x}[T]]$, $\bar{\mathbf{Y}}_k = [\bar{\mathbf{y}}_k[1], \dots, \bar{\mathbf{y}}_k[T]]$, and $\bar{\mathbf{Z}} = [\bar{\mathbf{z}}_k[1], \dots, \bar{\mathbf{z}}_k[t]]$, we have

$$\bar{\mathbf{Y}}_k = \hat{\mathbf{E}}_k \Phi_k \mathbf{G}_k \mathbf{X} + \bar{\mathbf{Z}}_k. \quad (8)$$

We suppose that each IRS k is aware of the channel matrix \mathbf{G}_k and the BS's transmitted signal \mathbf{X} via proper channel estimation and signalling from the BS. Accordingly, based on the received echo signal $\bar{\mathbf{Y}}_k$ in (8), each IRS k needs to estimate the DoA θ_k and the complex coefficient β_k as unknown parameters for the point target case, and needs to estimate the complete target response matrix $\hat{\mathbf{E}}_k$ for the extended target case.

III. ESTIMATION CRB DERIVATION

In this section, we derive the estimation CRB as the sensing performance metric for each IRS k to estimate the unknown parameters based on (8), which provides the variance lower bound for any unbiased estimators.

A. Point Target Case

For the point target case, the target response matrix $\hat{\mathbf{E}}_k$ is particularly specified by (4). Thus, the echo signal received at IRS k in (8) is re-expressed as

$$\bar{\mathbf{Y}}_k = \beta_k \mathbf{E}_k \Phi_k \mathbf{G}_k \mathbf{X} + \bar{\mathbf{Z}}_k, \quad (9)$$

where $\mathbf{E}_k = \tilde{\mathbf{a}}_k(\theta_k) \mathbf{a}_k^T(\theta_k)$. Let $\boldsymbol{\xi}_k = [\theta_k, \boldsymbol{\beta}_k]^T$ denote the three real parameters to be estimated, where $\boldsymbol{\beta}_k = [\text{Re}\{\beta_k\}, \text{Im}\{\beta_k\}]$. By vectorizing $\bar{\mathbf{Y}}_k$ in (9), we have

$$\tilde{\mathbf{y}}_k = \text{vec}(\bar{\mathbf{Y}}_k) = \tilde{\boldsymbol{\eta}}_k + \tilde{\mathbf{z}}_k, \quad (10)$$

where $\tilde{\boldsymbol{\eta}}_k = \text{vec}(\beta_k \mathbf{E}_k \Phi_k \mathbf{G}_k \mathbf{X})$ and $\tilde{\mathbf{z}}_k = \text{vec}(\bar{\mathbf{Z}}_k) \sim \mathcal{CN}(\mathbf{0}, \sigma_s^2 \mathbf{I}_{N_s T})$.

First, we derive the Fisher information matrix (FIM) $\mathbf{J}_k \in \mathbb{C}^{3 \times 3}$ for estimating the vector $\boldsymbol{\mu}$ from (10), which is given by [33]

$$[\mathbf{J}_k]_{l,p} = \frac{2}{\sigma_s^2} \text{Re} \left\{ \frac{\partial \tilde{\boldsymbol{\eta}}_k^H}{\partial [\boldsymbol{\xi}_k]_l} \frac{\partial \tilde{\boldsymbol{\eta}}_k}{\partial [\boldsymbol{\xi}_k]_p} \right\}, l, p \in \{1, 2, 3\}. \quad (11)$$

Recall that the statistic covariance matrix $\mathbf{R}_x = \sum_{k \in \mathcal{K}} \mathbf{W}_k + \mathbf{R}_0$ is also approximated as the sample covariance matrix at the BS. Based on (11), the FIM is derived in Lemma 1 as follows.

Lemma 1: The FIM \mathbf{J}_k for estimating $\boldsymbol{\xi}_k$ is given by

$$\mathbf{J}_k = \begin{bmatrix} J_{\theta_k, \theta_k} & \mathbf{J}_{\theta_k, \beta_k} \\ \mathbf{J}_{\theta_k, \beta_k}^T & \mathbf{J}_{\beta_k, \beta_k} \end{bmatrix}, \quad (12)$$

where

$$J_{\theta_k, \theta_k} = \frac{2T |\beta_k|^2}{\sigma_s^2} \text{tr} \left(\dot{\mathbf{E}}_k(\theta_k) \boldsymbol{\Phi}_k \mathbf{G}_k \mathbf{R}_x \mathbf{G}_k^H \boldsymbol{\Phi}_k^H \dot{\mathbf{E}}_k^H(\theta_k) \right), \quad (13)$$

$$\mathbf{J}_{\theta_k, \beta_k} = \frac{2T}{\sigma_s^2} \text{Re} \left\{ \beta_k^* \text{tr} \left(\mathbf{E}_k(\theta_k) \boldsymbol{\Phi}_k \mathbf{G}_k \mathbf{R}_x \mathbf{G}_k^H \boldsymbol{\Phi}_k^H \dot{\mathbf{E}}_k^H(\theta_k) \right) [1, j] \right\}, \quad (14)$$

$$\mathbf{J}_{\beta_k, \beta_k} = \frac{2T}{\sigma_s^2} \text{tr} \left(\mathbf{E}_k(\theta_k) \boldsymbol{\Phi}_k \mathbf{G}_k \mathbf{R}_x \mathbf{G}_k^H \boldsymbol{\Phi}_k^H \mathbf{E}_k^H(\theta_k) \right) \mathbf{I}_2, \quad (15)$$

with $\dot{\mathbf{E}}_k(\theta_k) = \frac{\partial \mathbf{E}_k}{\partial \theta_k}$ denoting the partial derivative of \mathbf{E}_k with respect to θ_k .

Proof: See Appendix A. ■

Next, based on the FIM \mathbf{J}_k , we are particularly interested in the CRB for each IRS k to estimate θ_k ,³ which is obtained as

$$\overline{\text{CRB}}_k(\theta_k) = [\mathbf{J}_k^{-1}]_{1,1} = \left[J_{\theta_k, \theta_k} - \mathbf{J}_{\theta_k, \tilde{\beta}_k} \mathbf{J}_{\tilde{\beta}_k, \tilde{\beta}_k}^{-1} \mathbf{J}_{\tilde{\beta}_k, \theta_k}^T \right]^{-1}. \quad (16)$$

For $\mathbf{E}_k = \tilde{\mathbf{a}}_k(\theta_k) \mathbf{a}_k^T(\theta_k)$, it follows that

$$\begin{aligned} \dot{\mathbf{E}}_k(\theta_k) &= \dot{\tilde{\mathbf{a}}}_k(\theta_k) \mathbf{a}_k^T(\theta_k) + \tilde{\mathbf{a}}_k(\theta_k) \dot{\mathbf{a}}_k^T(\theta_k) \\ &= j \frac{2\pi}{\lambda} d_s \cos(\theta_k) \left(\mathbf{D}_{N_s} \tilde{\mathbf{a}}_k(\theta_k) \mathbf{a}_k^T(\theta_k) + \tilde{\mathbf{a}}_k(\theta_k) \mathbf{a}_k^T(\theta_k) \mathbf{D}_N \right), \end{aligned} \quad (17)$$

where $\mathbf{D}_N = \text{diag}(0, 1, \dots, N-1)$. Based on (17) and (16), we have the following proposition.

Proposition 1: The CRB for each IRS to estimate θ_k is given by

$$\overline{\text{CRB}}_k(\theta_k) = \frac{\sigma_s^2}{2T |\beta_k|^2 \left(\text{tr} \left(\dot{\mathbf{E}}_k(\theta_k) \boldsymbol{\Phi}_k \mathbf{G}_k \mathbf{R}_x \mathbf{G}_k^H \boldsymbol{\Phi}_k^H \dot{\mathbf{E}}_k^H(\theta_k) \right) - \frac{|\text{tr}(\mathbf{E}_k(\theta_k) \boldsymbol{\Phi}_k \mathbf{G}_k \mathbf{R}_x \mathbf{G}_k^H \boldsymbol{\Phi}_k^H \dot{\mathbf{E}}_k^H(\theta_k))|^2}{\text{tr}(\mathbf{E}_k(\theta_k) \boldsymbol{\Phi}_k \mathbf{G}_k \mathbf{R}_x \mathbf{G}_k^H \boldsymbol{\Phi}_k^H \mathbf{E}_k^H(\theta_k))} \right)} \quad (18)$$

$$= \frac{\sigma_s^2 \lambda^2}{8T |\beta_k|^2 \pi^2 d_s^2 \cos^2(\theta_k) \left(\frac{(N_s-1)N_s(N_s+1)}{12} \text{tr}(\boldsymbol{\phi}_k^T \mathbf{U}_k \boldsymbol{\phi}_k^*) + N_s \text{tr}(\boldsymbol{\phi}_k^T \mathbf{D}_N \mathbf{U}_k \mathbf{D}_N \boldsymbol{\phi}_k^*) - \frac{N_s |\text{tr}(\boldsymbol{\phi}_k^T \mathbf{U}_k \mathbf{D}_N \boldsymbol{\phi}_k^*)|^2}{\text{tr}(\boldsymbol{\phi}_k^T \mathbf{U}_k \boldsymbol{\phi}_k^*)} \right)}, \quad (19)$$

where $\mathbf{U}_k = \mathbf{A}_k \mathbf{G}_k \mathbf{R}_x \mathbf{G}_k^H \mathbf{A}_k^H$ and $\mathbf{A}_k = \text{diag}(\mathbf{a}_k(\theta_k))$.

³As the complex coefficient β_k is affected by both the radar cross section and the round-trip pathloss, it is difficult for IRS k to extract target information from β_k . Therefore, only the CRB for estimating θ_k is considered.

Proof: See Appendix B. ■

Based on the closed-form CRB expression in (19), we have the following proposition.

Proposition 2: When the number of sensing elements N_s at each IRS becomes sufficiently large, the CRB of estimating θ_k for the point target case decreases inversely proportional to the cubic of N_s , i.e., $\text{CRB}_k(\theta_k) \propto \frac{1}{N_s^3}$.

Proof: See Appendix C. ■

B. Extended Target Case

Next, we consider the extended target case, in which the objective of each IRS k is to estimate the complete target response matrix $\hat{\mathbf{E}}_k \in \mathbb{C}^{N_s \times N}$. By vectorizing the received echo signal in (8) at IRS k , we have

$$\hat{\mathbf{y}}_k = \text{vec}(\bar{\mathbf{Y}}_k) = \hat{\boldsymbol{\eta}}_k + \tilde{\mathbf{z}}_k, \quad (20)$$

where

$$\hat{\boldsymbol{\eta}}_k = \text{vec}(\hat{\mathbf{E}}_k \Phi_k \mathbf{G}_k \mathbf{X}) = ((\Phi_k \mathbf{G}_k \mathbf{X})^T \otimes \mathbf{I}_{N_s}) \hat{\mathbf{h}}_k, \quad (21)$$

and $\hat{\mathbf{h}}_k = \text{vec}(\hat{\mathbf{E}}_k)$. Based on the definition of FIM in (11) and the received echo signal model in (21), the FIM for estimating $\hat{\mathbf{h}}_k$ is given in the following lemma.

Lemma 2: The FIM \mathbf{F}_k for estimating $\hat{\mathbf{h}}_k$ from (10) is given by

$$\mathbf{F}_k = \begin{bmatrix} \mathbf{F}_{\text{Re}\{\hat{\mathbf{h}}_k\}, \text{Re}\{\hat{\mathbf{h}}_k\}} & \mathbf{F}_{\text{Re}\{\hat{\mathbf{h}}_k\}, \text{Im}\{\hat{\mathbf{h}}_k\}} \\ \mathbf{F}_{\text{Im}\{\hat{\mathbf{h}}_k\}, \text{Re}\{\hat{\mathbf{h}}_k\}} & \mathbf{F}_{\text{Im}\{\hat{\mathbf{h}}_k\}, \text{Im}\{\hat{\mathbf{h}}_k\}} \end{bmatrix}, \quad (22)$$

where

$$\mathbf{F}_{\text{Re}\{\hat{\mathbf{h}}_k\}, \text{Re}\{\hat{\mathbf{h}}_k\}} = \mathbf{F}_{\text{Im}\{\hat{\mathbf{h}}_k\}, \text{Im}\{\hat{\mathbf{h}}_k\}} = \frac{2}{\sigma_s^2} \text{Re} \{ (\Phi_k \mathbf{G}_k \mathbf{X})^* (\Phi_k \mathbf{G}_k \mathbf{X})^T \otimes \mathbf{I}_{N_s} \}, \quad (23)$$

$$\mathbf{F}_{\text{Re}\{\hat{\mathbf{h}}_k\}, \text{Im}\{\hat{\mathbf{h}}_k\}} = -\mathbf{F}_{\text{Im}\{\hat{\mathbf{h}}_k\}, \text{Re}\{\hat{\mathbf{h}}_k\}} = \frac{2}{\sigma_s^2} \text{Re} \{ (\Phi_k \mathbf{G}_k \mathbf{X})^* (\Phi_k \mathbf{G}_k \mathbf{X})^T \otimes \mathbf{I}_{N_s} \}. \quad (24)$$

Proof: See Appendix D. ■

Based on (22), we have the following proposition.

Proposition 3: The CRB for estimation the target response matrix $\hat{\mathbf{E}}_k$ by IRS k is given by

$$\begin{aligned} \widetilde{\text{CRB}}_k(\hat{\mathbf{E}}_k) &= \text{tr}(\mathbf{F}_k^{-1}) = \frac{N_s \sigma_s^2}{T} \text{tr} \left((\Phi_k^* \mathbf{G}_k^* \mathbf{R}_x^* \mathbf{G}_k^T \Phi_k^T)^{-1} \right) \\ &= \frac{N_s \sigma_s^2}{T} \text{tr} \left((\mathbf{G}_k \mathbf{R}_x^H \mathbf{G}_k^H)^{-1} \right). \end{aligned} \quad (25)$$

Proof: This proposition can be verified following a similar procedure as in [6, (11)]. Therefore, the detailed proof is omitted for brevity. ■

It is observed from (25) that the $\widetilde{\text{CRB}}_k(\hat{\mathbf{E}}_k)$ only depends on the transmit covariance \mathbf{R}_x or the transmit beamformers. Besides, the condition $M \geq \text{rank}(\mathbf{R}_x) \geq N \geq \text{rank}(\mathbf{G}_k)$ must hold to ensure $\widetilde{\text{CRB}}_k(\hat{\mathbf{E}}_k)$ to be bounded, such that the target response matrix $\hat{\mathbf{E}}_k$ is estimable. Moreover, we have the following proposition to reveal the relationship between CRB and the number of sensors N_s at each IRS.

Proposition 4: When the number of sensing elements N_s at each IRS becomes sufficiently large, the CRB of estimating $\hat{\mathbf{E}}_k$ for the extended target case increases proportional to N_s , i.e., $\widetilde{\text{CRB}}_k(\hat{\mathbf{E}}_k) \propto N_s$.

Proof: See Appendix E. ■

By comparing Propositions 2 versus 4, it is observed that deploying more reflecting elements at IRS is beneficial to enhance the performance for target AoA estimation (in terms of lower CRB) for the point target case, but leads to higher CRB for the extended target case. This is due to the fact that higher array gain can be exploited for sensing in the former case, but more target parameters need to be estimated in the latter case.

IV. JOINT BEAMFORMING FOR CRB MINIMIZATION WITH POINT TARGETS

In this section, we jointly optimize the transmit beamforming at the BS and the reflective beamforming at the multiple IRSs to minimize the estimation CRB $\overline{\text{CRB}}_k(\theta_k)$ in (19) for the point target case, subject to the maximum transmit power constraint at the BS and the SINR requirements at individual CUs. To ensure the fair optimization of sensing performance, we particularly minimize the maximum CRB among the K IRSs. As such, for Type-I and Type-II CU receivers, the SINR-constrained max-CRB minimization problems are formulated as (P1-I)

and (P1-II), respectively.

$$\begin{aligned} \text{(P1-I)} : \quad & \min_{\{\mathbf{W}_k\}, \{\Phi_k\}, \mathbf{R}_0} \max_{k \in \mathcal{K}} \overline{\text{CRB}}_k(\theta_k) \\ & \text{s.t.} \quad \gamma_k^{(\text{I})}(\{\mathbf{W}_k\}, \{\Phi_k\}, \mathbf{R}_0) \geq \Gamma_k, \forall k \in \mathcal{K} \end{aligned} \quad (26a)$$

$$\text{tr} \left(\sum_{k \in \mathcal{K}} \mathbf{W}_k + \mathbf{R}_0 \right) \leq P_{\text{sum}} \quad (26b)$$

$$\mathbf{R}_0 \succeq \mathbf{0} \quad (26c)$$

$$\mathbf{W}_k \succeq \mathbf{0}, \forall k \in \mathcal{K} \quad (26d)$$

$$\text{rank}(\mathbf{W}_k) = 1, \forall k \in \mathcal{K} \quad (26e)$$

$$|\phi_{k,n}| = 1, \forall n \in \mathcal{N}, \forall k \in \mathcal{K}. \quad (26f)$$

$$\begin{aligned} \text{(P1-II)} : \quad & \min_{\{\mathbf{W}_k\}, \{\Phi_k\}, \mathbf{R}_0} \max_{k \in \mathcal{K}} \overline{\text{CRB}}_k(\theta_k) \\ & \text{s.t.} \quad \gamma_k^{(\text{II})}(\{\mathbf{W}_k\}, \{\Phi_k\}, \mathbf{R}_0) \geq \Gamma_k, \forall k \in \mathcal{K} \end{aligned} \quad (27a)$$

(26b), (26c), (26d), (26e), and (26f).

In problems (P1-I) and (P1-II), (26a), (26b) and (26f) denote the SINR constraints at the CUs, the transmit power constraint at the BS, and the unit-modular constraints at the IRSs, respectively.

Notice that problems (P1-I) and (P1-II) are both non-convex. This is due to the fact that their objective functions are non-convex and the SINR constraints in (26a) and (27a), the unit-modulus constraints in (26f), and the rank-one constraints in (26e) are all non-convex. To tackle the non-convexity, we propose alternating-optimization-based algorithms to solve them, in which the transmit beamforming $\{\mathbf{W}_k\}/\mathbf{R}_0$ at the BS and the reflective beamforming $\{\Phi_k\}$ at IRSs are optimized in an alternating manner. Note that problems (P1-I) and (P1-II) are similar, with the only difference lying on the SINR $\gamma_k^{(\text{I})}$ in (2) for Type-I receivers versus $\gamma_k^{(\text{II})}$ in (3) for Type-II receivers. As a result, the proposed algorithm for solving problem (P1-I) can be directly generalized to solve (P1-II) by replacing $\gamma_k^{(\text{II})}$ with $\gamma_k^{(\text{I})}$. In the following, we focus on solving problem (P1-I), and omit the details for solving (P1-II). In the following, we obtain the optimal transmit beamformers $\{\mathbf{W}_k\}$ and \mathbf{R}_0 for problem (P1-I) under given fixed reflective beamformers $\{\Phi_k\}$ in Section IV-A, and then optimize $\{\Phi_k\}$ for (P1-I) under given $\{\mathbf{W}_k\}$ and $\{\mathbf{R}_0\}$ in Section IV-B.

A. Optimal Transmit Beamforming to (P1-I) with Given Reflective Beamforming

First, we aim to optimize the transmit beamforming $\{\mathbf{W}_k\}$ and \mathbf{R}_0 at the BS with given $\{\Phi_k\}$, for which the optimization problem is expressed as

$$\begin{aligned} \text{(P2)} : \quad & \min_{\{\mathbf{W}_k\}, \mathbf{R}_0} \max_{k \in \mathcal{K}} \overline{\text{CRB}}_k(\theta_k) \\ \text{s.t.} \quad & \text{(26a), (26b), (26c), (26d) and (26e)}. \end{aligned}$$

In (P2), we use the CRB formula in (19) for transmit beamforming optimization. Note that problem (P2) is still non-convex due to the non-convexity of the objective function, the SINR constraints in (26a), and the rank constraints in (26e). In the following, we use the SDR technique to find the optimal solution.

First, we define $\tilde{\mathbf{G}}_k = \mathbf{G}_k^H \Phi_k^H \mathbf{h}_k \mathbf{h}_k^H \Phi_k \mathbf{G}_k$, and equivalently express the SINR constraints in (26a) as

$$\frac{1}{\Gamma_k} \text{tr} \left(\tilde{\mathbf{G}}_k \mathbf{W}_k \right) \geq \sum_{k' \in \mathcal{K} \setminus k} \text{tr} \left(\tilde{\mathbf{G}}_k \mathbf{W}_{k'} \right) + \text{tr} \left(\tilde{\mathbf{G}}_k \mathbf{R}_0 \right) + \sigma_k^2, \forall k \in \mathcal{K}. \quad (29)$$

Furthermore, it is observed from (19) that $\overline{\text{CRB}}_k(\theta_k) = \frac{\kappa}{f_{2,k}(\{\mathbf{W}_k\}, \mathbf{R}_0) - f_{3,k}(\{\mathbf{W}_k\}, \mathbf{R}_0)}$, where $\kappa = \frac{\sigma_s^2 \lambda^2}{8T|\beta_k|^2 \pi^2 d_s^2 \cos^2(\theta_k)}$ is a constant, and

$$\begin{aligned} f_{2,k}(\{\mathbf{W}_k\}, \mathbf{R}_0) &= \frac{(N_s - 1) N_s (N_s + 1)}{12} \text{tr} \left(\phi_k^T \mathbf{B}_k \left(\sum_{k \in \mathcal{K}} \mathbf{W}_k + \mathbf{R}_0 \right) \mathbf{B}_k^H \phi_k^* \right) \\ &+ N_s \text{tr} \left(\phi_k^T \mathbf{D}_N \mathbf{B}_k \left(\sum_{k \in \mathcal{K}} \mathbf{W}_k + \mathbf{R}_0 \right) \mathbf{B}_k^H \mathbf{D}_N \phi_k^* \right), \end{aligned} \quad (30)$$

$$f_{3,k}(\{\mathbf{W}_k\}, \mathbf{R}_0) = \frac{N_s \left| \text{tr} \left(\phi_k^T \mathbf{B}_k \left(\sum_{k \in \mathcal{K}} \mathbf{W}_k + \mathbf{R}_0 \right) \mathbf{B}_k^H \mathbf{D}_N \phi_k^* \right) \right|^2}{\text{tr} \left(\phi_k^T \mathbf{B}_k \left(\sum_{k \in \mathcal{K}} \mathbf{W}_k + \mathbf{R}_0 \right) \mathbf{B}_k^H \phi_k^* \right)}, \quad (31)$$

with $\mathbf{B}_k = \mathbf{A}_k \mathbf{G}_k$. As such, problem (P2) is can be equivalently solved via solving the following problem:

$$\begin{aligned} \text{(P2.1)} : \quad & \max_{\{\mathbf{W}_k\}, \mathbf{R}_0} \min_{k \in \mathcal{K}} f_{2,k}(\{\mathbf{W}_k\}, \mathbf{R}_0) - f_{3,k}(\{\mathbf{W}_k\}, \mathbf{R}_0) \\ \text{s.t.} \quad & \text{(26b), (26c), (26d), (26e), and (29)}. \end{aligned}$$

To solve problem (P2.1), we introduce the auxiliary variables $\tilde{\nu}_1$ and $\{\tilde{\nu}_{2,k}\}$. Accordingly, problem (P2.1) is equivalently reformulated as

$$(P2.2) : \begin{aligned} & \max_{\substack{\{\mathbf{W}_k\}, \mathbf{R}_0, \\ \tilde{\nu}_1, \{\tilde{\nu}_{2,k}\}}} \tilde{\nu}_1 \\ & \text{s.t.} \quad f_{2,k}(\{\mathbf{W}_k\}, \mathbf{R}_0) - \tilde{\nu}_{2,k} \geq \tilde{\nu}_1, \forall k \in \mathcal{K} \end{aligned} \quad (33a)$$

$$\tilde{\nu}_1 \geq 0 \quad (33b)$$

$$\tilde{\nu}_{2,k} \geq f_{3,k}(\{\mathbf{W}_k\}, \mathbf{R}_0), \forall k \in \mathcal{K} \quad (33c)$$

$$(26b), (26c), (26d), (26e), \text{ and } (29).$$

To deal with the non-convex constraints in (33c), we transform them into a set of linear matrix inequality (LMI) constraints in (34) base on the Schur's complement.

$$\left[\begin{array}{cc} \text{tr} \left(\phi_k^T \mathbf{B}_k \left(\sum_{k \in \mathcal{K}} \mathbf{W}_k + \mathbf{R}_0 \right) \mathbf{B}_k^H \phi_k^* \right) & \sqrt{N_s} \text{tr} \left(\phi_k^T \mathbf{B}_k \left(\sum_{k \in \mathcal{K}} \mathbf{W}_k + \mathbf{R}_0 \right) \mathbf{B}_k^H \mathbf{D}_N \phi_k^* \right) \\ \sqrt{N_s} \text{tr} \left(\phi_k^T \mathbf{D}_N \mathbf{B}_k \left(\sum_{k \in \mathcal{K}} \mathbf{W}_k^H + \mathbf{R}_0^H \right) \mathbf{B}_k^H \phi_k^* \right) & \tilde{\nu}_{2,k} \end{array} \right] \succeq 0, \forall k \in \mathcal{K}. \quad (34)$$

As a result, problem (P2.2) is equivalent to the following convex problem:

$$(P2.3) : \begin{aligned} & \max_{\substack{\{\mathbf{W}_k\}, \mathbf{R}_0, \\ \tilde{\nu}_1, \{\tilde{\nu}_{2,k}\}}} \tilde{\nu}_1 \\ & \text{s.t.} \quad (26b), (26c), (26d), (26e), (29), (33a), (33b), \text{ and } (34). \end{aligned}$$

Furthermore, we remove the rank constraints in (26e), and accordingly obtain the relaxed version of (P2.3) as (SDR2.3). Note that (SDR2.3) is a convex semi-definite program (SDP), which can be optimally solved by convex solvers such as CVX [34]. Let $\{\overline{\mathbf{W}}_k\}$ and $\overline{\mathbf{R}}_0$ denote the obtained optimal solution to (SDR2.3). As the obtained optimal solution $\{\overline{\mathbf{W}}_k\}$ may not be of rank-one, we construct the optimal rank-one solutions of $\{\overline{\mathbf{W}}_k^*\}$ and the corresponding $\overline{\mathbf{R}}_0^*$ to problem (P2.3) and thus (P2) by using the following proposition.

Proposition 5: Based on the obtained optimal solution $\{\overline{\mathbf{W}}_k\}$ and $\overline{\mathbf{R}}_0$ to (SDR2.3), the optimal solution to problem (P2.3) and (P2) is given by

$$\overline{\mathbf{W}}_k^* = \overline{\mathbf{w}}_k \overline{\mathbf{w}}_k^H, \forall k \in \mathcal{K}, \quad (36)$$

with $\overline{\mathbf{w}}_k = \left(\tilde{\mathbf{h}}_k^H \overline{\mathbf{W}}_k \tilde{\mathbf{h}}_k \right)^{-\frac{1}{2}} \overline{\mathbf{W}}_k \tilde{\mathbf{h}}_k$, where $\tilde{\mathbf{h}}_k^H = \mathbf{h}_k^H \Phi_k \mathbf{G}_k$, and the corresponding optimal solution of $\overline{\mathbf{R}}_0^*$ is given by

$$\overline{\mathbf{R}}_0^* = \overline{\mathbf{R}}_0 + \sum_{k \in \mathcal{K}} \overline{\mathbf{W}}_k - \sum_{k \in \mathcal{K}} \overline{\mathbf{W}}_k^*. \quad (37)$$

Proof: See Appendix F. ■

It is shown in Proposition 5 that the solutions $\{\overline{\mathbf{W}}_k^*\}$ and $\overline{\mathbf{R}}_0^*$ in (36) and (37) are actually optimal for problem (SDR2.2). Therefore, the SDR is tight between (P2.2) and (SDR2.2), and thus we obtain the optimal solution to (P2).

B. Reflective Beamforming Optimization for (P1-I) with Given Transmit Beamforming

Next, we optimize the reflective beamforming $\{\Phi_k\}$ or $\{\phi_k\}$ for problem (P1-I) with given $\{\mathbf{w}_k\}$ and \mathbf{R}_0 . In this case, the optimization problem is expressed as

$$\begin{aligned} \text{(P3)} : \quad & \min_{\{\phi_k\}} \max_{k \in \mathcal{K}} \overline{\text{CRB}}_k(\theta_k) \\ & \text{s.t.} \quad (26a), (26f), \end{aligned}$$

in which we use the CRB formulas in (19) for reflective beamforming optimization. Notice that problem (P3) can be equivalently decomposed into K subproblems given by

$$\begin{aligned} \text{(P3.1.k)} : \quad & \max_{\phi_k} \frac{(N_s - 1) N_s (N_s + 1)}{12} \text{tr}(\phi_k^T \mathbf{U}_k \phi_k^*) + N_s \text{tr}(\phi_k^T \mathbf{D}_N \mathbf{U}_k \mathbf{D}_N \phi_k^*) \\ & - \frac{N_s |\text{tr}(\phi_k^T \mathbf{U}_k \mathbf{D}_N \phi_k^*)|^2}{\text{tr}(\phi_k^T \mathbf{U}_k \phi_k^*)} \\ & \text{s.t.} \quad (26a), (26f). \end{aligned}$$

Problem (P3.1.k) is still non-convex due to the non-convexity of the objective function, the SINR constraints in (26a), and the unit-modulus constraints in (26f).

In the following, we use the SDR technique to handle problem (P3.1.k). Towards this end, we define $\mathbf{H}_k = \text{diag}(\mathbf{h}_k^H)$ and $\Theta_k = \phi_k^* \phi_k^T$, where $\Theta_k \succeq \mathbf{0}$ and $\text{rank}(\Theta_k) = 1, \forall k \in \mathcal{K}$. Then, the SINR at CU k becomes

$$\tilde{\gamma}_k^{(1)}(\{\Theta_k\}) = \frac{\text{tr}(\mathbf{H}_k \mathbf{G}_k \mathbf{w}_k \mathbf{w}_k^H \mathbf{G}_k^H \mathbf{H}_k^H \Theta_k)}{\sum_{k' \in \mathcal{K} \setminus k} \text{tr}(\mathbf{H}_k \mathbf{G}_k \mathbf{w}_{k'} \mathbf{w}_{k'}^H \mathbf{G}_k^H \mathbf{H}_k^H \Theta_k) + \text{tr}(\mathbf{H}_k \mathbf{G}_k \mathbf{R}_0 \mathbf{G}_k^H \mathbf{H}_k^H \Theta_k) + \sigma_k^2}. \quad (40)$$

By substituting (40) into the constraints in (26a) and skipping the rank-one constraints, problem (P3.1.k) is relaxed as

$$\begin{aligned}
(\text{SDR3.1.k}) : \quad & \max_{\Theta_k} \frac{(N_s - 1) N_s (N_s + 1)}{12} \text{tr}(\mathbf{U}_k \Theta_k) + N_s \text{tr}(\mathbf{D}_N \mathbf{U}_k \mathbf{D}_N \Theta_k) \\
& - \frac{N_s |\text{tr}(\mathbf{U}_k \mathbf{D}_N \Theta_k)|^2}{\text{tr}(\mathbf{U}_k \Theta_k)} \\
\text{s.t.} \quad & \sum_{k' \in \mathcal{K} \setminus k} \text{tr}(\mathbf{H}_k \mathbf{G}_k \mathbf{w}_{k'} \mathbf{w}_{k'}^H \mathbf{G}_k^H \mathbf{H}_k^H \Theta_k) \\
& + \text{tr}(\mathbf{H}_k \mathbf{G}_k \mathbf{R}_0 \mathbf{G}_k^H \mathbf{H}_k^H \Theta_k) + \sigma_k^2 \\
& - \frac{1}{\Gamma_k} \text{tr}(\mathbf{H}_k \mathbf{G}_k \mathbf{w}_k \mathbf{w}_k^H \mathbf{G}_k^H \mathbf{H}_k^H \Theta_k) \leq 0 \tag{41a} \\
& [\Theta_k]_{n,n} = 1, n \in \mathcal{N} \tag{41b} \\
& \Theta_k \succeq \mathbf{0}. \tag{41c}
\end{aligned}$$

Furthermore, by introducing an auxiliary variable τ_k , problem (SDR3.1.k) is equivalently re-expressed as

$$\begin{aligned}
(\text{SDR3.2.k}) : \quad & \max_{\Theta_k, \tau_k} \frac{(N_s - 1) N_s (N_s + 1)}{12} \text{tr}(\mathbf{U}_k \Theta_k) + N_s \text{tr}(\mathbf{D}_N \mathbf{U}_k \mathbf{D}_N \Theta_k) - \tau_k \\
\text{s.t.} \quad & \begin{bmatrix} \tau_k & \sqrt{N_s} \text{tr}(\mathbf{U}_k \mathbf{D}_N \Theta_k) \\ \sqrt{N_s} \text{tr}(\Theta_k^H \mathbf{D}_N \mathbf{U}_k^H) & \text{tr}(\mathbf{U}_k \Theta_k) \end{bmatrix} \succeq \mathbf{0} \tag{42a} \\
& (41a), (41b), \text{ and } (41c).
\end{aligned}$$

Here, the constraints in (42a) is obtained from $\tau_k \geq \frac{N_s |\text{tr}(\mathbf{U}_k \mathbf{D}_N \Theta_k)|^2}{\text{tr}(\mathbf{U}_k \Theta_k)}$ by using Schur's complement. Note that problem (SDR3.2.k) is a convex SDP which can be optimally solved by CVX. Let Θ_k^* denote the obtained optimal solution to (SDR3.2.k).

Notice that the obtained solution Θ_k^* may not be of rank-one, and as a result, it may not be the optimal solution to problem (P3.1.k) or (P3). To tackle this issue, we further use the Gaussian randomization to construct a high-quality solution to problem (P3.1.k) based on the obtained $\{\Theta_k^*\}$. Specifically, we first generate a number of randomly vectors $\mathbf{r}_k \sim \mathcal{CN}(\mathbf{0}, \mathbf{I}_N)$, and then construct a number of rank-one solutions as

$$\phi_k = e^{j \arg \left\{ (\Theta_k^*)^{\frac{1}{2}} \mathbf{r}_k \right\}}. \tag{43}$$

Then, we find the desirable solution of ϕ_k that minimizes $\overline{\text{CRB}}_k(\theta_k)$ among all random generated ϕ_k 's. As a result, problem (P3) is finally solved.

In summary, the alternating-optimization-based algorithm for solving (P1-I) is implemented by solving problems (P2) and (P3) alternately. Notice that problem (P2) is optimally solved and the solution to (P3) would lead to a decreasing max-CRB with a sufficient number of Gaussian randomizations. As such, the alternating optimization leads to monotonically non-increasing max-CRB values over iterations, and thus is ensured to converge. Furthermore, the alternating-optimization-based algorithm can be performed in a distributed way in practice. In particular, in each iteration, the BS can first optimize the transmit beamforming by solving problem (P2), and then each IRS can optimize its own reflective beamforming by solving problem (P3.1.k) in a distributed manner. This is thus very efficient in practical implementation.

V. JOINT BEAMFORMING FOR CRB MINIMIZATION WITH EXTENDED TARGETS

In this section, we jointly optimize the transmit beamforming $\{\mathbf{W}_k\}$ and \mathbf{R}_0 at the BS and the reflective beamforming $\{\Phi_k\}$ at the IRSs to minimize the maximum estimation CRB among the IRSs, subject to the maximum transmit power constraint at the BS and the SINR requirements at individual CUs. For Type-I and Type-II CU receivers, the SINR-constrained max-CRB minimization problems are formulated as (P4-I) and (P4-II) in the following, respectively.

$$\begin{aligned} \text{(P4-I)} : \quad & \min_{\{\mathbf{W}_k\}, \{\Phi_k\}, \mathbf{R}_0} \max_{k \in \mathcal{K}} \widetilde{\text{CRB}}_k(\hat{\mathbf{E}}_k) \\ & \text{s.t.} \quad (26\text{a}), (26\text{b}), (26\text{c}), (26\text{d}), (26\text{e}), \text{ and } (26\text{f}). \end{aligned}$$

$$\begin{aligned} \text{(P4-II)} : \quad & \min_{\{\mathbf{W}_k\}, \{\Phi_k\}, \mathbf{R}_0} \max_{k \in \mathcal{K}} \widetilde{\text{CRB}}_k(\hat{\mathbf{E}}_k) \\ & \text{s.t.} \quad (27\text{a}), (26\text{b}), (26\text{c}), (26\text{d}), (26\text{e}), \text{ and } (26\text{f}). \end{aligned}$$

Problems (P4-I) and (P4-II) are both non-convex. This is due to the fact that their objective functions, the SINR constraints in (26a) and (27a), the unit-modulus constraints in (26f), and the rank-one constraints in (26e) are all non-convex. To tackle the non-convexity, we propose an alternating-optimization-based algorithm to solve them by optimizing $\{\mathbf{W}_k\}/\mathbf{R}_0$ and $\{\Phi_k\}$ alternately. Notice that problems (P4-I) and (P4-II) have similar structures. Therefore, in the following, we only focus on solving problem (P4-I) and omit the details for solving (P4-II).

A. Optimal Transmit Beamforming to (P4-I) with Given Reflective Beamforming

First, we aim to optimize the transmit beamforming $\{\mathbf{W}_k\}$ and dedicated signal covariance \mathbf{R}_0 with given $\{\Phi_k\}$. In this case, the optimization problem is formulated as

$$\begin{aligned} \text{(P5)} : \quad & \min_{\{\mathbf{W}_k\}, \mathbf{R}_0} \max_{k \in \mathcal{K}} \widetilde{\text{CRB}}_k(\hat{\mathbf{E}}_k) \\ & \text{s.t.} \quad (26a), (26b), (26c), (26d), \text{ and } (26e). \end{aligned}$$

By introducing an auxiliary variable \tilde{u} , problem (P5) is equivalent to the following problem.

$$\begin{aligned} \text{(P5.1)} : \quad & \min_{\{\mathbf{W}_k\}, \mathbf{R}_0, \tilde{u}} \quad \tilde{u} \\ & \text{s.t.} \quad \tilde{u} \geq \frac{N_s \sigma_s^2}{T} \text{tr} \left(\left(\mathbf{G}_k \left(\sum_{k=1}^K \mathbf{W}_k + \mathbf{R}_0 \right) \mathbf{G}_k^H \right)^{-1} \right), \forall k \quad (47a) \\ & \quad (26b), (26c), (26d), (26e), \text{ and } (29). \end{aligned}$$

We then use the SDR technique to handle problem (P5.1). By removing the rank-one constraints in (26e), we obtain the relaxed version of (P5.1) as (SDR5.1). Note that problem (SDR5.1) is a convex SDP problem that can be solved by CVX. Let $\{\widetilde{\mathbf{W}}_k\}$ and $\widetilde{\mathbf{R}}_0$ denote the obtained optimal solution to problem (SDR5.1). The optimal rank-one solution $\{\widetilde{\mathbf{W}}_k^*\}$ and the corresponding $\widetilde{\mathbf{R}}_0^*$ to problems (P5) and (P5.1) can be constructed via the following proposition.

Proposition 6: Based on the obtained optimal solution $\{\widetilde{\mathbf{W}}_k\}$ and $\widetilde{\mathbf{R}}_0$ to (SDR5.1), the optimal solution of $\{\mathbf{W}_k\}$ to problem (P5) and (P5.1) is given by

$$\widetilde{\mathbf{W}}_k^* = \tilde{\mathbf{w}}_k \tilde{\mathbf{w}}_k^H, \forall k \in \mathcal{K}, \quad (48)$$

with $\tilde{\mathbf{w}}_k = \left(\tilde{\mathbf{h}}_k^H \widetilde{\mathbf{W}}_k \tilde{\mathbf{h}}_k \right)^{-\frac{1}{2}} \widetilde{\mathbf{W}}_k \tilde{\mathbf{h}}_k$, and the corresponding \mathbf{R}_0^* is given by

$$\widetilde{\mathbf{R}}_0^* = \widetilde{\mathbf{R}}_0 + \sum_{k \in \mathcal{K}} \widetilde{\mathbf{W}}_k - \sum_{k \in \mathcal{K}} \widetilde{\mathbf{W}}_k^*. \quad (49)$$

Proof: The proof is similar to that of Proposition 5, and thus is omitted. ■

B. Reflective Beamforming Optimization for (P4-I) with Given Transmit Beamforming

Next, we optimize the reflecting coefficients $\{\phi_k\}$ in problem (P4-I) with given $\{\mathbf{W}_k\}$ and \mathbf{R}_0 . Note that the objective function is independent of $\{\phi_k\}$. As a result, any $\{\phi_k\}$ that guarantee the SINR constraints in (26a) is a feasible solution to problem (P4-I). As the reflective beamformers $\{\phi_k\}$ may affect the optimization of $\{\mathbf{W}_k\}$ and \mathbf{R}_0 by changing the achieved maximum SINR,

we propose to optimize $\{\phi_k\}$ to maximize the SINR at CUs for expanding the feasible region of problem (P5). Note that the SINR of each CU k only depends on its corresponding IRS k . Therefore, we optimize the reflective beamforming at each IRS k to maximize the SINR at the corresponding CU k . The corresponding optimization problem becomes

$$\begin{aligned}
 \text{(P6)} : \quad & \max_{\Phi_k} \frac{|\mathbf{h}_k^H \Phi_k \mathbf{G}_k \mathbf{w}_k|^2}{\sum_{k' \neq k}^K |\mathbf{h}_k^H \Phi_k \mathbf{G}_k \mathbf{w}_{k'}|^2 + \mathbf{h}_k^H \Phi_k \mathbf{G}_k \mathbf{R}_0 \mathbf{G}_k^H \Phi_k^H \mathbf{h}_k + \sigma_k^2} \\
 \text{s.t.} \quad & (26f).
 \end{aligned}$$

Furthermore, by replacing the objective function in problem (P6) by $\tilde{\gamma}_k^{(1)}$ in (40) and skipping the rank-one constraints on Θ_k , we have a relaxed version of (P6) as

$$\begin{aligned}
 \text{(SDR6)} : \quad & \max_{\Theta_k} \frac{\text{tr}(\mathbf{H}_k \mathbf{G}_k \mathbf{w}_k \mathbf{w}_k^H \mathbf{G}_k^H \mathbf{H}_k^H \Theta_k)}{\sum_{k' \neq k}^K \text{tr}(\mathbf{H}_k \mathbf{G}_k \mathbf{w}_{k'} \mathbf{w}_{k'}^H \mathbf{G}_k^H \mathbf{H}_k^H \Theta_k) + \text{tr}(\mathbf{H}_k \mathbf{G}_k \mathbf{R}_0 \mathbf{G}_k^H \mathbf{H}_k^H \Theta_k) + \sigma_k^2} \\
 \text{s.t.} \quad & [\Theta_k]_{n,n} = 1, n = 1, \dots, N \tag{51a}
 \end{aligned}$$

$$\Theta_k \succeq \mathbf{0}. \tag{51b}$$

Problem (SDR6) is still a non-convex problem as the objective function is non-convex. To tackle this issue, we define

$$\mathbf{T}_1 = \mathbf{H}_k \mathbf{G}_k \mathbf{w}_k \mathbf{w}_k^H \mathbf{G}_k^H \mathbf{H}_k^H, \tag{52}$$

$$\mathbf{T}_2 = \sum_{k' \neq k}^K \mathbf{H}_k \mathbf{G}_k \mathbf{w}_{k'} \mathbf{w}_{k'}^H \mathbf{G}_k^H \mathbf{H}_k^H + \mathbf{H}_k \mathbf{G}_k \mathbf{R}_0 \mathbf{G}_k^H \mathbf{H}_k^H. \tag{53}$$

Then, problem (SDR6) is equivalent to the following optimization problem:

$$\begin{aligned}
 \text{(SDR6.1)} : \quad & \max_{\Theta_k} \frac{\text{tr}(\mathbf{T}_1 \Theta_k)}{\text{tr}(\mathbf{T}_2 \Theta_k) + \sigma_k^2} \\
 \text{s.t.} \quad & [\Theta_k]_{n,n} = 1, n = 1, \dots, N \tag{54a}
 \end{aligned}$$

$$\Theta_k \succeq \mathbf{0}. \tag{54b}$$

By further defining $\mathbf{M}_k = \frac{\Theta_k}{\text{tr}(\mathbf{T}_2 \Theta_k) + \sigma_k^2}$ and $t_k = \frac{1}{\text{tr}(\mathbf{T}_2 \Theta_k) + \sigma_k^2}$, we transform the optimization of Θ_k as that of \mathbf{M}_k and t_k . As such, problem (SDR6.1) is transformed into the following problem:

$$\begin{aligned}
(\text{SDR6.2}) : \quad & \max_{\mathbf{M}_k, t_k} \quad \text{tr}(\mathbf{T}_1 \mathbf{M}_k) \\
& \text{s.t.} \quad [\mathbf{M}_k]_{n,n} - t_k = 0, n = 1, \dots, N
\end{aligned} \tag{55a}$$

$$\mathbf{M}_k \succeq \mathbf{0} \tag{55b}$$

$$t_k \geq 0 \tag{55c}$$

$$\text{tr}(\mathbf{T}_2 \mathbf{M}_k) + \sigma_k^2 t_k = 1. \tag{55d}$$

Note that the problem (SDR6.2) is an SDP problem and can be solved by CVX. Let \mathbf{M}_k^* and t_k^* denote the obtained optimal solution to (SDR6.2). Then, the optimal solution Θ_k^* to (SDR6) is calculated by $\Theta_k^* = \frac{\mathbf{M}_k^*}{t_k^*}$. Now, it remains to find a high-quality solution to (P6). As the obtained solution Θ_k^* may not be of rank-one, it may not be the optimal solution to problem (P6). To overcome this case, the Gaussian randomization method is used to construct a high-quality rank-one solution to problems (P6). Similar to (43), we first generate a number of random vectors $\mathbf{r}_k \sim \mathcal{CN}(\mathbf{0}, \mathbf{I}_N)$, and construct a number of rank-one candidates as $\phi_k = e^{j \arg\left\{(\Theta_k^*)^{\frac{1}{2}} \mathbf{r}_k\right\}}$. Then, we find the desirable solution of ϕ_k that maximizes the objective function in problem (P6) among all randomly generated ϕ_k 's. As a result, problem (P6) is finally solved.

In summary, the alternating-optimization-based algorithm for solving (P4-I) is implemented by solving problems (P5) and (P6) alternately. Similarly as for (P1-I), the alternating optimization leads to monotonically non-increasing max-CRB values for problem (P4-I) over iterations, and thus is ensured to converge. Furthermore, the alternating-optimization-based algorithm can also be performed in a distributed way in practice.

VI. NUMERICAL RESULTS

This section provides numerical results to validate the effectiveness of our proposed designs. In the simulation, we set the carrier frequency as 6 GHz and the bandwidth as 1 MHz. We adopt the Rician fading channel model with the K-factor being 5 dB for wireless channels between the BS and the IRSs and those between the IRSs and the CUs. We also set the noise power spectrum density as -174 dBm/Hz, the SINR constraints to be $\Gamma_k = \Gamma, \forall k \in \mathcal{K}$, and the radar dwell time as $T = 100$. In particular, we consider that there are one BS and two IRSs as shown in Fig. 2, which are located at $[0, 0]$ meters (m), $[-30, 30]$ m, and $[30, 30]$ m, respectively. Their

associated CUs are located at $[-35, 25]$ m and $[30, 25]$ m, and targets are located at $[-35, 22]$ m and $[35, 27]$ m, respectively. For comparison, we consider the following benchmark schemes:

- **Transmit beamforming (BF) only:** The IRSs implement random reflection coefficients. Accordingly, we only optimize the transmit beamforming at the BS, e.g., by solving problems (P2) for the point target case and by solving problem (P5) for the extended target case, when the Type-I CU receivers are implemented.
- **ZF-BF:** First, we design the transmit information beamformers based on the ZF principle. In particular, by defining $\tilde{\mathbf{H}} = [\tilde{\mathbf{h}}_1, \dots, \tilde{\mathbf{h}}_K]$ and $\tilde{\mathbf{W}}^{\text{ZF}} = \tilde{\mathbf{H}} \left(\tilde{\mathbf{H}}^H \tilde{\mathbf{H}} \right)^{-1}$, we set the ZF beamformer for each CU k as $\mathbf{w}_k^{\text{ZF}} = \sqrt{p_k} \frac{\tilde{\mathbf{w}}_k^{\text{ZF}}}{\|\tilde{\mathbf{w}}_k^{\text{ZF}}\|}$, where $\tilde{\mathbf{w}}_k^{\text{ZF}}$ denotes the k -th column of $\tilde{\mathbf{W}}^{\text{ZF}}$ and p_k is the transmit power for CU k . Next, we optimize the transmit power $\{p_k\}$, the sensing beamformers \mathbf{R}_0 , and the reflective beamformers $\{\Phi_k\}$ by alternating optimization, similarly as in Sections IV and V for point and extended targets, respectively.
- **Sensing only:** This schemes corresponds to the proposed design without SINR constraints for communications, by equivalently setting $\Gamma_k = 0, \forall k \in \mathcal{K}$, in problems (P1-I), (P1-II), (P4-I), and (P4-II) for the four considered cases, respectively. This thus serves as performance upper bound for our proposed design, in terms of the lower bound of the estimation CRB.

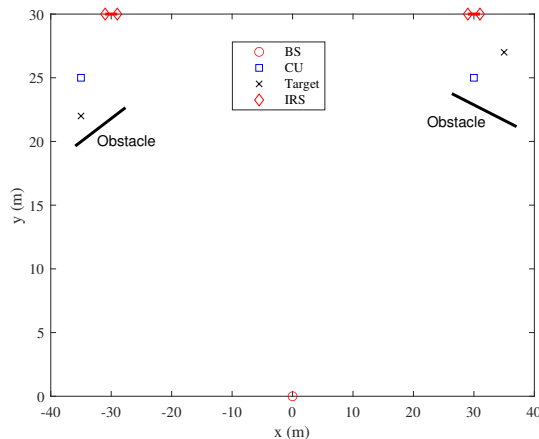


Fig. 2. The location topology.

Fig. 3 shows the achieved max-CRB versus the maximum transmit power P_{sum} at the BS for the point target case, where we set $\Gamma = 10$ dB. It is observed that our proposed design performs close to the performance upper bound by the sensing only scheme, and outperforms other benchmark schemes over the whole regime of P_{sum} . It is also observed that the proposed

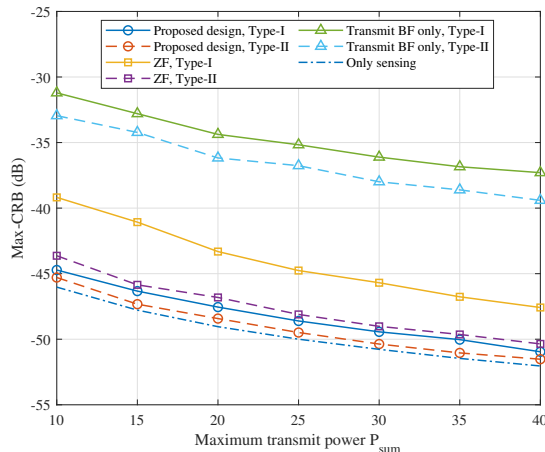


Fig. 3. The achieved max-CRB versus the maximum transmit power P_{sum} with $\Gamma = 10$ dB and $M = N = N_s = 8$.

design with Type-II receivers achieves lower CRB than that with Type-I receivers. This shows the benefits of sensing-signal-interference cancellation. In particular, it is shown in simulations that for problem (P1-II) with Type-II receivers, the obtained \mathbf{R}_0 is always non-zero for facilitating sensing without interfering with CU receivers; while for problem (P1-I) with Type-I receivers, the obtained \mathbf{R}_0 is generally zero for avoiding the interference towards CU receivers.

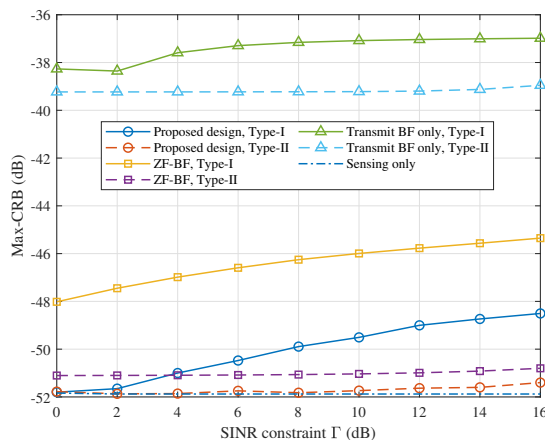


Fig. 4. The achieved max-CRB versus the SINR constraint with $P_{\text{sum}} = 40$ W and $M = N = N_s = 8$.

Fig. 4 shows the achieved max-CRB versus the SINR constraint Γ at each CU for the point target case. It is observed that in the low SINR regime, the performance achieved by our proposed design with both types of CU receivers is close to that by the sensing only scheme. As the SINR constraint increases, the performance gap between the proposed design with Type-II CU receivers and that with Type-I CU receivers is observed to increase. This is due to the fact that when the SINR constraint becomes large, the BS needs to allocate more transmit power to the information

signals, which may suffer from more severe interference from dedicated sensing signals when Type-I CU receivers are employed. This shows that the sensing-interference cancellation of Type-II receivers are particularly appealing when both communication and sensing requirements become stringent.

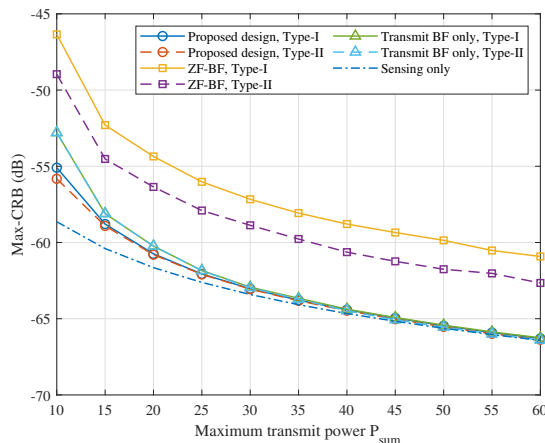


Fig. 5. The minimum CRB versus the maximum transmit power P_{sum} with $\Gamma = 20$ dB and $M = N = N_s = 8$.

Fig. 5 shows the achieved max-CRB versus the maximum transmit power P_{sum} at the BS for extended target case, where we set $\Gamma = 20$ dB. It is observed that our proposed design performs most close to the performance upper bound by the sensing only scheme, and outperforms the transmit beamforming only scheme and ZF beamforming scheme especially when the maximum transmit power P_{sum} is low. As the maximum transmit power P_{sum} increases, the CRB performances by our proposed design and the transmit beamforming only scheme gradually approach the performance upper bound. This is due to the fact that the CRB performance mainly depends on the BS transmit beamforming optimization when the maximum transmit power is high. It is also observed that the proposed design with Type-II receivers achieves lower CRB than that with Type-I receivers when the transmit power is low. It shows that performing the sensing interference cancellation is less significant for the extended target case than that for the point target case.

Fig. 6 shows the achieved max-CRB versus the SINR constraint Γ at each CU for extended target case. It is observed that in the low SINR regime, the performance achieved by our proposed design with both two types of CU receivers is close to that by the sensing only scheme. This phenomenon is similar to the point target case. It is also observed that the ZF beamforming scheme performs worst among all schemes. This is different from the observation for the point

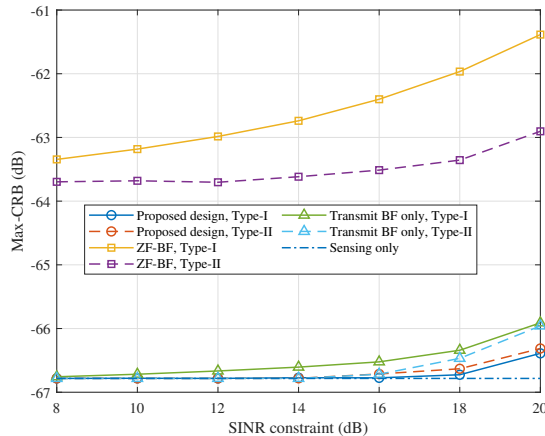


Fig. 6. The minimum CRB versus the SINR requirements with $P_{\text{sum}} = 40$ W and $M = N = N_s = 8$.

target case, which indicates the importance of transmit beamforming optimization for minimizing the max-CRB in the extended target case.

VII. CONCLUSION

This paper studied a multi-IRS-enabled ISAC system, in which multiple semi-passive IRSs are deployed to provide ISAC services at separate areas. We derived the closed-form CRBs for each IRS to estimate target parameters based on the ISAC signals, by considering two cases with point and extended targets, respectively. These derived CRBs provides insights on the multi-semi-passive-IRS-enabled sensing. Furthermore, we proposed two efficient joint transmit and reflective beamforming designs to minimize the maximum CRB at all IRSs while ensuring the communication requirements, by considering two different types of CU receivers. Numerical results showed the effectiveness of our proposed designs, as compared to various benchmarks without such joint optimization. It was also shown that the sensing signal interference cancellation at Type-II receivers is essential in further enhancing the ISAC performance, especially for the point target case.

APPENDIX A

PROOF OF LEMMA 1

According to (11), we have the following the partial derivations:

$$\frac{\partial \tilde{\eta}}{\partial \theta_k} = \beta_k \text{vec} \left(\dot{\mathbf{E}}_k(\theta_k) \Phi_k \mathbf{G}_k \mathbf{X} \right), \quad (56)$$

$$\frac{\partial \tilde{\eta}}{\partial \beta_k} = [1, j] \otimes \text{vec} \left(\mathbf{E}_k \Phi_k \mathbf{G}_k \mathbf{X} \right), \quad (57)$$

where $\dot{\mathbf{E}}_k(\theta_k) = \frac{\partial \mathbf{E}_k}{\partial \theta_k}$ denotes the partial derivative of \mathbf{E}_k with respect to θ_k . Consequently, the elements of FIM in (11) are given by

$$\begin{aligned} J_{\theta_k, \theta_k} &= \frac{2}{\sigma_s^2} \text{Re} \left\{ \left(\beta_k \text{vec} \left(\dot{\mathbf{E}}_k(\theta_k) \Phi_k \mathbf{G}_k \mathbf{X} \right) \right)^H \beta_k \text{vec} \left(\dot{\mathbf{E}}_k(\theta_k) \Phi_k \mathbf{G}_k \mathbf{X} \right) \right\} \\ &= \frac{2|\beta_k|^2}{\sigma_s^2} \text{Re} \left\{ \text{tr} \left(\left(\dot{\mathbf{E}}_k(\theta_k) \Phi_k \mathbf{G}_k \mathbf{X} \right)^H \dot{\mathbf{E}}_k(\theta_k) \Phi_k \mathbf{G}_k \mathbf{X} \right) \right\} \\ &= \frac{2T|\beta_k|^2}{\sigma_s^2} \text{tr} \left(\dot{\mathbf{E}}_k(\theta_k) \Phi_k \mathbf{G}_k \mathbf{R}_x \mathbf{G}_k^H \Phi_k^H \dot{\mathbf{E}}_k^H(\theta_k) \right), \end{aligned} \quad (58)$$

$$\begin{aligned} \mathbf{J}_{\theta_k, \beta_k} &= \frac{2}{\sigma_s^2} \text{Re} \left\{ \left(\beta_k \text{vec} \left(\dot{\mathbf{E}}_k(\theta_k) \Phi_k \mathbf{G}_k \mathbf{X} \right) \right)^H [1, j] \otimes \text{vec} \left(\mathbf{E}_k \Phi_k \mathbf{G}_k \mathbf{X} \right) \right\} \\ &= \frac{2T}{\sigma_s^2} \text{Re} \left\{ \beta_k^* \text{tr} \left(\mathbf{E}_k(\theta_k) \Phi_k \mathbf{G}_k \mathbf{R}_x \mathbf{G}_k^H \Phi_k^H \dot{\mathbf{E}}_k^H(\theta_k) \right) [1, j] \right\}, \end{aligned} \quad (59)$$

$$\begin{aligned} \mathbf{J}_{\beta_k, \beta_k} &= \frac{2}{\sigma_s^2} \text{Re} \left\{ ([1, j] \otimes \text{vec} \left(\mathbf{E}_k \Phi_k \mathbf{G}_k \mathbf{X} \right))^H [1, j] \otimes \text{vec} \left(\mathbf{E}_k \Phi_k \mathbf{G}_k \mathbf{X} \right) \right\} \\ &= \frac{2T}{\sigma_s^2} \text{Re} \left\{ [1, j]^H [1, j] (\text{vec} \left(\mathbf{E}_k \Phi_k \mathbf{G}_k \mathbf{X} \right))^H \text{vec} \left(\mathbf{E}_k \Phi_k \mathbf{G}_k \mathbf{X} \right) \right\} \\ &= \frac{2T}{\sigma_s^2} \text{tr} \left(\mathbf{E}_k(\theta_k) \Phi_k \mathbf{G}_k \mathbf{R}_x \mathbf{G}_k^H \Phi_k^H \mathbf{E}_k^H(\theta_k) \right) \mathbf{I}_2. \end{aligned} \quad (60)$$

Therefore, Lemma 1 is finally proved.

APPENDIX B
PROOF OF PROPOSITION 1

First, by substituting (13)-(15) into (16), we obtain (18). Then, we substitute (17) into (13)-(15) to obtain the following results:

$$\begin{aligned}
\dot{\mathbf{E}}_k(\theta_k) \Phi_k \mathbf{G}_k \mathbf{R}_x \mathbf{G}_k^H \Phi_k^H \dot{\mathbf{E}}_k^H(\theta_k) &= \\
\frac{4\pi^2 d_s^2 \cos^2(\theta_k)}{\lambda^2} (\mathbf{D}_{N_s} \tilde{\mathbf{a}}_k(\theta_k) \mathbf{a}_k^T(\theta_k) + \tilde{\mathbf{a}}_k(\theta_k) \mathbf{a}_k^T(\theta_k) \mathbf{D}_N) \Phi_k \mathbf{G}_k \mathbf{R}_x \mathbf{G}_k^H \Phi_k^H \\
&\cdot (\mathbf{a}_k^*(\theta_k) \tilde{\mathbf{a}}_k^H(\theta_k) \mathbf{D}_{N_s} + \mathbf{D}_N \mathbf{a}_k^*(\theta_k) \tilde{\mathbf{a}}_k^H(\theta_k)) \\
&= \frac{4\pi^2 d_s^2 \cos^2(\theta_k)}{\lambda^2} \left(\frac{(N_s - 1) N_s (2N_s - 1)}{6} \text{tr}(\phi_k^T \mathbf{U}_k \phi_k^*) + \frac{(N_s - 1) N_s}{2} \text{tr}(\phi_k^T \mathbf{U}_k \mathbf{D}_N \phi_k^*) \right. \\
&\left. + \frac{(N_s - 1) N_s}{2} \text{tr}(\phi_k^T \mathbf{D}_N \mathbf{U}_k \phi_k^*) + N_s \text{tr}(\phi_k^T \mathbf{D}_N \mathbf{U}_k \mathbf{D}_N \phi_k^*) \right), \tag{61}
\end{aligned}$$

$$\begin{aligned}
\mathbf{E}_k(\theta_k) \Phi_k \mathbf{G}_k \mathbf{R}_x \mathbf{G}_k^H \Phi_k^H \dot{\mathbf{E}}_k^H(\theta_k) &= \\
j \frac{2\pi}{\lambda} d_s \cos(\theta_k) \tilde{\mathbf{a}}_k(\theta_k) \mathbf{a}_k^T(\theta_k) \Phi_k \mathbf{G}_k \mathbf{R}_x \mathbf{G}_k^H \Phi_k^H (\mathbf{a}_k^*(\theta_k) \tilde{\mathbf{a}}_k^H(\theta_k) \mathbf{D}_{N_s} + \mathbf{D}_N \mathbf{a}_k^*(\theta_k) \tilde{\mathbf{a}}_k^H(\theta_k)) \\
&= j \frac{2\pi}{\lambda} d_s \cos(\theta_k) \left(\frac{(N_s - 1) N_s}{2} \text{tr}(\phi_k^T \mathbf{U}_k \phi_k^*) + N_s \text{tr}(\phi_k^T \mathbf{U}_k \mathbf{D}_N \phi_k^*) \right), \tag{62}
\end{aligned}$$

$$\begin{aligned}
\mathbf{E}_k(\theta_k) \Phi_k \mathbf{G}_k \mathbf{R}_x \mathbf{G}_k^H \Phi_k^H \mathbf{E}_k^H(\theta_k) &= \\
\tilde{\mathbf{a}}_k(\theta_k) \mathbf{a}_k^T(\theta_k) \Phi_k \mathbf{G}_k \mathbf{R}_x \mathbf{G}_k^H \Phi_k^H \mathbf{a}_k^*(\theta_k) \tilde{\mathbf{a}}_k^H(\theta_k) &= N_s \text{tr}(\phi_k^T \mathbf{U}_k \phi_k^*), \tag{63}
\end{aligned}$$

where $\mathbf{U}_k = \mathbf{A}_k \mathbf{G}_k \mathbf{R}_x \mathbf{G}_k^H \mathbf{A}_k^H$ and $\mathbf{A}_k = \text{diag}(\mathbf{a}_k(\theta_k))$. Substituting (61)-(63) into (18) yields Proposition 1.

APPENDIX C
PROOF OF PROPOSITION 2

Based on the closed-form CRB in (19) and by considering N_s to be sufficiently large, we have

$$\begin{aligned}
\lim_{N_s \rightarrow \infty} N_s^3 \text{CRB}(\theta_k) &= \frac{N_s^3 \sigma_s^2 \lambda^2}{8T |\beta_k|^2 \pi^2 d_s^2 \cos^2(\theta_k) \left(\frac{(N_s - 1) N_s (N_s + 1)}{12} \text{tr}(\phi_k^T \mathbf{U}_k \phi_k^*) \right)} \\
&= \frac{3\sigma_s^2 \lambda^2}{2T |\beta_k|^2 \pi^2 d_s^2 \cos^2(\theta_k) \text{tr}(\phi_k^T \mathbf{U}_k \phi_k^*)}. \tag{64}
\end{aligned}$$

Therefore, $\lim_{N_s \rightarrow \infty} N_s^3 \text{CRB}(\theta_k)$ equal to a determined value independent of N_s . As a result, Proposition 2 is proved.

APPENDIX D

PROOF OF LEMMA 2

We first decomposed the estimation parameter $\hat{\mathbf{h}}_k$ into real and imaginary parts that are denoted by $\text{Re}\{\hat{\mathbf{h}}_k\}$ and $\text{Im}\{\hat{\mathbf{h}}_k\}$, respectively. As a result, the FIM is equivalently expressed as

$$\mathbf{F}_k = \begin{bmatrix} \mathbf{F}_{\text{Re}\{\hat{\mathbf{h}}_k\}, \text{Re}\{\hat{\mathbf{h}}_k\}} & \mathbf{F}_{\text{Re}\{\hat{\mathbf{h}}_k\}, \text{Im}\{\hat{\mathbf{h}}_k\}} \\ \mathbf{F}_{\text{Im}\{\hat{\mathbf{h}}_k\}, \text{Re}\{\hat{\mathbf{h}}_k\}} & \mathbf{F}_{\text{Im}\{\hat{\mathbf{h}}_k\}, \text{Im}\{\hat{\mathbf{h}}_k\}} \end{bmatrix}. \quad (65)$$

Then, we derive each part in the FIM as

$$\begin{aligned} \mathbf{F}_{\text{Re}\{\hat{\mathbf{h}}_k\}, \text{Re}\{\hat{\mathbf{h}}_k\}} &= \frac{2}{\sigma_s^2} \text{Re} \left\{ \frac{\partial \tilde{\boldsymbol{\eta}}_k^H}{\partial \text{Re}\{\hat{\mathbf{h}}_k\}} \frac{\partial \tilde{\boldsymbol{\eta}}_k}{\partial \text{Re}\{\hat{\mathbf{h}}_k\}} \right\} \\ &= \frac{2}{\sigma_s^2} \text{Re} \left\{ \left((\boldsymbol{\Phi}_k \mathbf{G}_k \mathbf{X})^T \otimes \mathbf{I}_{N_s} \right)^H \left((\boldsymbol{\Phi}_k \mathbf{G}_k \mathbf{X})^T \otimes \mathbf{I}_{N_s} \right) \right\} \\ &= \frac{2}{\sigma_s^2} \text{Re} \left\{ (\boldsymbol{\Phi}_k \mathbf{G}_k \mathbf{X})^* (\boldsymbol{\Phi}_k \mathbf{G}_k \mathbf{X})^T \otimes \mathbf{I}_{N_s} \right\}, \end{aligned} \quad (66)$$

$$\begin{aligned} \mathbf{F}_{\text{Im}\{\hat{\mathbf{h}}_k\}, \text{Im}\{\hat{\mathbf{h}}_k\}} &= \frac{2}{\sigma_s^2} \text{Re} \left\{ \frac{\partial \tilde{\boldsymbol{\eta}}_k^H}{\partial \text{Im}\{\hat{\mathbf{h}}_k\}} \frac{\partial \tilde{\boldsymbol{\eta}}_k}{\partial \text{Im}\{\hat{\mathbf{h}}_k\}} \right\} \\ &= \frac{2}{\sigma_s^2} \text{Re} \left\{ \left((\boldsymbol{\Phi}_k \mathbf{G}_k \mathbf{X})^T \otimes \mathbf{I}_{N_s} \right)^H \left((\boldsymbol{\Phi}_k \mathbf{G}_k \mathbf{X})^T \otimes \mathbf{I}_{N_s} \right) \right\} \\ &= \frac{2}{\sigma_s^2} \text{Re} \left\{ (\boldsymbol{\Phi}_k \mathbf{G}_k \mathbf{X})^* (\boldsymbol{\Phi}_k \mathbf{G}_k \mathbf{X})^T \otimes \mathbf{I}_{N_s} \right\}, \end{aligned} \quad (67)$$

$$\begin{aligned} \mathbf{F}_{\text{Re}\{\hat{\mathbf{h}}_k\}, \text{Im}\{\hat{\mathbf{h}}_k\}} &= -\mathbf{F}_{\text{Im}\{\hat{\mathbf{h}}_k\}, \text{Re}\{\hat{\mathbf{h}}_k\}} = \frac{2}{\sigma_s^2} \text{Im} \left\{ \frac{\partial \tilde{\boldsymbol{\eta}}_k^H}{\partial \text{Re}\{\hat{\mathbf{h}}_k\}} \frac{\partial \tilde{\boldsymbol{\eta}}_k}{\partial \text{Im}\{\hat{\mathbf{h}}_k\}} \right\} \\ &= \frac{2}{\sigma_s^2} \text{Re} \left\{ \left((\boldsymbol{\Phi}_k \mathbf{G}_k \mathbf{X})^T \otimes \mathbf{I}_{N_s} \right)^H \left((\boldsymbol{\Phi}_k \mathbf{G}_k \mathbf{X})^T \otimes \mathbf{I}_{N_s} \right) \right\} \\ &= \frac{2}{\sigma_s^2} \text{Re} \left\{ (\boldsymbol{\Phi}_k \mathbf{G}_k \mathbf{X})^* (\boldsymbol{\Phi}_k \mathbf{G}_k \mathbf{X})^T \otimes \mathbf{I}_{N_s} \right\}. \end{aligned} \quad (68)$$

As a result, the Lemma 2 is obtained.

APPENDIX E

PROOF OF PROPOSITION 4

Based on the closed-form CRB in (25) and by considering N_s to be sufficiently large, we have

$$\lim_{N_s \rightarrow \infty} \frac{\widetilde{\text{CRB}}_k(\hat{\mathbf{E}}_k)}{N_s} = \frac{\sigma_s^2}{T} \text{tr} \left((\mathbf{G}_k^* \mathbf{R}_x^* \mathbf{G}_k^T)^{-1} \right). \quad (69)$$

Thus, $\lim_{N_s \rightarrow \infty} \frac{\widetilde{\text{CRB}}_k(\hat{\mathbf{E}}_k)}{N_s}$ is equal to a constant value independent of N_s . As a result, Proposition 4 is proved.

APPENDIX F
PROOF OF PROPOSITION 5

First, we have

$$\begin{aligned} \frac{1}{\Gamma_k} \tilde{\mathbf{h}}_k^H \overline{\mathbf{W}}_k^* \tilde{\mathbf{h}}_k &= \frac{1}{\Gamma_k} \tilde{\mathbf{h}}_k^H \overline{\mathbf{W}}_k \tilde{\mathbf{h}}_k \\ &\geq \sum_{k' \neq k}^K \tilde{\mathbf{h}}_k^H \overline{\mathbf{W}}_{k'} \tilde{\mathbf{h}}_k + \tilde{\mathbf{h}}_k^H \overline{\mathbf{R}}_0 \tilde{\mathbf{h}}_k + \sigma_k^2 = \sum_{k' \neq k}^K \tilde{\mathbf{h}}_k^H \overline{\mathbf{W}}_{k'}^* \tilde{\mathbf{h}}_k + \tilde{\mathbf{h}}_k^H \overline{\mathbf{R}}_0^* \tilde{\mathbf{h}}_k + \sigma_k^2, \forall k. \end{aligned} \quad (70)$$

As a result, the SINR constraints in (26a) are still satisfied with (36)-(37). Furthermore, for any $\mathbf{z} \in \mathbb{C}^{M \times 1}$, it holds that

$$\mathbf{z}^H \left(\overline{\mathbf{W}}_k - \overline{\mathbf{W}}_k^* \right) \mathbf{z} = \mathbf{z}^H \overline{\mathbf{W}}_k \mathbf{z} - \left| \mathbf{z}^H \overline{\mathbf{W}}_k \tilde{\mathbf{h}}_k \right|^2 \left(\tilde{\mathbf{h}}_k^H \overline{\mathbf{W}}_k \tilde{\mathbf{h}}_k \right)^{-1}. \quad (71)$$

According to the Cauchy-Schwarz inequality, we have

$$\left| \mathbf{z}^H \overline{\mathbf{W}}_k \tilde{\mathbf{h}}_k \right|^2 \leq \left(\mathbf{z}^H \overline{\mathbf{W}}_k \mathbf{z} \right) \left(\tilde{\mathbf{h}}_k^H \overline{\mathbf{W}}_k \tilde{\mathbf{h}}_k \right), \quad (72)$$

and thus $\mathbf{z}^H \left(\overline{\mathbf{W}}_k - \overline{\mathbf{W}}_k^* \right) \mathbf{z} \geq 0$ also holds. As a result, we have $\overline{\mathbf{W}}_k - \overline{\mathbf{W}}_k^* \succeq 0$, i.e., $\overline{\mathbf{W}}_k - \overline{\mathbf{W}}_k^*$ is positive semidefinite. Therefore, it follows that $\overline{\mathbf{R}}_0^*$ is also positive semi-definite. As a result, $\{\overline{\mathbf{W}}_k^*\}$ and $\overline{\mathbf{R}}_0^*$ are optimal to problem (P1.1). This completes the proof.

REFERENCES

- [1] Y. Cui, F. Liu, X. Jing, and J. Mu, "Integrating sensing and communications for ubiquitous IoT: Applications, trends, and challenges," *IEEE Netw.*, vol. 35, no. 5, pp. 158–167, Sep. 2021.
- [2] F. Liu, Y. Cui, C. Masouros, J. Xu, T. X. Han, Y. C. Eldar, and S. Buzzi, "Integrated sensing and communications: Towards dual-functional wireless networks for 6G and beyond," *IEEE J. Sel. Areas Commun.*, vol. 40, no. 6, pp. 1728–1767, Jun. 2022.
- [3] Y. Huang, Y. Fang, X. Li, and J. Xu, "Coordinated power control for network integrated sensing and communication," *IEEE Trans. Veh. Technol.*, vol. 71, no. 12, pp. 13 361–13 365, Dec. 2022.
- [4] Z. Lyu, G. Zhu, and J. Xu, "Joint maneuver and beamforming design for UAV-enabled integrated sensing and communication," *IEEE Trans. Wireless Commun.*, vol. 22, no. 4, pp. 2424–2440, Apr. 2023.
- [5] H. Hua, J. Xu, and T. X. Han, "Optimal transmit beamforming for integrated sensing and communication," *IEEE Trans. Veh. Technol.*, vol. 22, no. 4, pp. 2278–2294, Mar. 2023.
- [6] F. Liu, Y.-F. Liu, A. Li, C. Masouros, and Y. C. Eldar, "Cramér-Rao bound optimization for joint radar-communication beamforming," *IEEE Trans. Signal Process.*, vol. 70, pp. 240–253, Dec. 2022.
- [7] C. Huang, A. Zappone, G. C. Alexandropoulos, M. Debbah, and C. Yuen, "Reconfigurable intelligent surfaces for energy efficiency in wireless communication," *IEEE Trans. Wireless Commun.*, vol. 18, no. 8, pp. 4157–4170, 2019.
- [8] M. Di Renzo, A. Zappone, M. Debbah, M.-S. Alouini, C. Yuen, J. De Rosny, and S. Tretyakov, "Smart radio environments empowered by reconfigurable intelligent surfaces: How it works, state of research, and the road ahead," *IEEE J. Sel. Areas Commun.*, vol. 38, no. 11, pp. 2450–2525, Nov. 2020.

- [9] Q. Wu, S. Zhang, B. Zheng, C. You, and R. Zhang, "Intelligent reflecting surface-aided wireless communications: A tutorial," *IEEE Trans. Commun.*, vol. 69, no. 5, pp. 3313–3351, May 2021.
- [10] H. Xie, J. Xu, and Y.-F. Liu, "Max-min fairness in IRS-aided multi-cell MISO systems with joint transmit and reflective beamforming," *IEEE Trans. Wireless Commun.*, vol. 20, no. 2, pp. 1379–1393, Feb. 2021.
- [11] C. Pan, G. Zhou, K. Zhi, S. Hong, T. Wu, Y. Pan, H. Ren, M. Di Renzo, A. L. Swindlehurst, R. Zhang, and A. Y. Zhang, "An overview of signal processing techniques for RIS/IRS-aided wireless systems," *IEEE J. Sel. Topics Signal Process.*, vol. 16, no. 5, pp. 883–917, Aug. 2022.
- [12] H. Li, S. Shen, and B. Clerckx, "Beyond diagonal reconfigurable intelligent surfaces: A multi-sector mode enabling highly directional full-space wireless coverage," *early access in IEEE J. Sel. Areas Commun.*, 2023.
- [13] S. Buzzi, E. Grossi, M. Lops, and L. Venturino, "Foundations of MIMO radar detection aided by reconfigurable intelligent surfaces," *IEEE Trans. Signal Process.*, vol. 70, pp. 1749–1763, Mar. 2022.
- [14] R. Liu, M. Li, H. Luo, Q. Liu, and A. L. Swindlehurst, "Integrated sensing and communication with reconfigurable intelligent surfaces: Opportunities, applications, and future directions," *IEEE Wireless Commun.*, vol. 30, no. 1, pp. 50–57, Feb. 2023.
- [15] X. Song, J. Xu, F. Liu, T. X. Han, and Y. C. Eldar, "Intelligent reflecting surface enabled sensing: Cramér-Rao bound optimization," *IEEE Trans. Signal Process.*, vol. 71, pp. 2011–2026, 2023.
- [16] X. Shao, C. You, W. Ma, X. Chen, and R. Zhang, "Target sensing with intelligent reflecting surface: Architecture and performance," *IEEE J. Sel. Areas Commun.*, vol. 40, no. 7, pp. 2070–2084, Jul. 2022.
- [17] X. Wang, Z. Fei, Z. Zheng, and J. Guo, "Joint waveform design and passive beamforming for RIS-assisted dual-functional radar-communication system," *IEEE Trans. Veh. Technol.*, vol. 70, no. 5, pp. 5131–5136, May 2021.
- [18] X. Song, D. Zhao, H. Hua, T. X. Han, X. Yang, and J. Xu, "Joint transmit and reflective beamforming for IRS-assisted integrated sensing and communication," in *Proc. IEEE WCNC*, 2022, pp. 189–194.
- [19] R. Liu, M. Li, Y. Liu, Q. Wu, and Q. Liu, "Joint transmit waveform and passive beamforming design for RIS-aided DFRC systems," *IEEE J. Sel. Topics Signal Process.*, vol. 16, no. 5, pp. 995–1010, Aug. 2022.
- [20] M. Hua, Q. Wu, C. He, S. Ma, and W. Chen, "Joint active and passive beamforming design for IRS-aided radar-communication," *IEEE Trans. Wireless Commun.*, vol. 22, no. 4, pp. 2278–2294, Apr. 2023.
- [21] X. Li, J. Fang, F. Gao, and H. Li, "Joint active and passive beamforming for intelligent reflecting surface-assisted massive MIMO systems," 2019. [Online]. Available: <https://arxiv.org/pdf/2207.05611.pdf>
- [22] Z. Yang, M. Chen, W. Saad, W. Xu, M. Shikh-Bahaei, H. V. Poor, and S. Cui, "Energy-efficient wireless communications with distributed reconfigurable intelligent surfaces," *IEEE Trans. Wireless Commun.*, vol. 21, no. 1, pp. 665–679, Jan. 2022.
- [23] T. V. Nguyen, D. N. Nguyen, M. Di Renzo, and R. Zhang, "Leveraging secondary reflections and mitigating interference in multi-IRS/RIS aided wireless networks," *IEEE Trans. Wireless Commun.*, vol. 22, no. 1, pp. 502–517, Jan. 2023.
- [24] C. Huang, Z. Yang, G. C. Alexandropoulos, K. Xiong, L. Wei, C. Yuen, Z. Zhang, and M. Debbah, "Multi-hop RIS-empowered terahertz communications: A DRL-based hybrid beamforming design," *IEEE J. Sel. Areas Commun.*, vol. 39, no. 6, pp. 1663–1677, Jun. 2021.
- [25] R. Liang, J. Fan, J. Luo, and J. Joung, "A multi-route cascaded IRSs beamforming scheme for mmWave communication systems," *IEEE Trans. Veh. Technol.*, vol. 71, no. 6, pp. 6813–6818, Jun. 2022.
- [26] W. Mei and R. Zhang, "Cooperative beam routing for multi-IRS aided communication," *IEEE Wireless Commun. Lett.*, vol. 10, no. 2, pp. 426–430, Feb. 2021.
- [27] —, "Multi-beam multi-hop routing for intelligent reflecting surfaces aided massive MIMO," *IEEE Trans. Wireless Commun.*, vol. 21, no. 3, pp. 1897–1912, Mar. 2022.

- [28] W. Mei, B. Zheng, C. You, and R. Zhang, "Intelligent reflecting surface-aided wireless networks: From single-reflection to multireflection design and optimization," *Proc. IEEE*, vol. 110, no. 9, pp. 1380–1400, May 2022.
- [29] R. Sankar, S. P. Chepuri, and Y. C. Eldar, "Beamforming in integrated sensing and communication systems with reconfigurable intelligent surfaces," 2022. [Online]. Available: <https://arxiv.org/abs/2206.07679>
- [30] B. Zheng, C. You, W. Mei, and R. Zhang, "A survey on channel estimation and practical passive beamforming design for intelligent reflecting surface aided wireless communications," *IEEE Commun. Surv. Tuts.*, vol. 24, no. 2, pp. 1035–1071, Feb. 2022.
- [31] C.-Y. Chen and P. P. Vaidyanathan, "MIMO radar waveform optimization with prior information of the extended target and clutter," *IEEE Trans. Signal Process.*, vol. 57, no. 9, pp. 3533–3544, Sep. 2009.
- [32] J. W. Koch, "Bayesian approach to extended object and cluster tracking using random matrices," *IEEE Trans. Aerosp. Electron. Syst.*, vol. 44, no. 3, pp. 1042–1059, Jul. 2008.
- [33] S. M. Kay, *Fundamentals of Statistical Signal Processing: Estimation Theory*. Cliffs, NJ, USA: Prentice-Hall., 1993.
- [34] M. Grant and S. Boyd, "CVX: Matlab software for disciplined convex programming, version 2.1," 2014.